5.1 Ring Fibre Laser Configuration

Figure 5.1 shows the ring fibre laser configuration of the GO-based erbium-doped fibre laser. An isolator ensures unidirectional light propagation. The polarization controller (PC) is to maintain the polarization state of the light after each round trip propagation and thus improving output pulse stability. The cavity length is ~12.7 m. To optimize the laser performance of pulse operation, output coupler with transmittance of 10% is used.

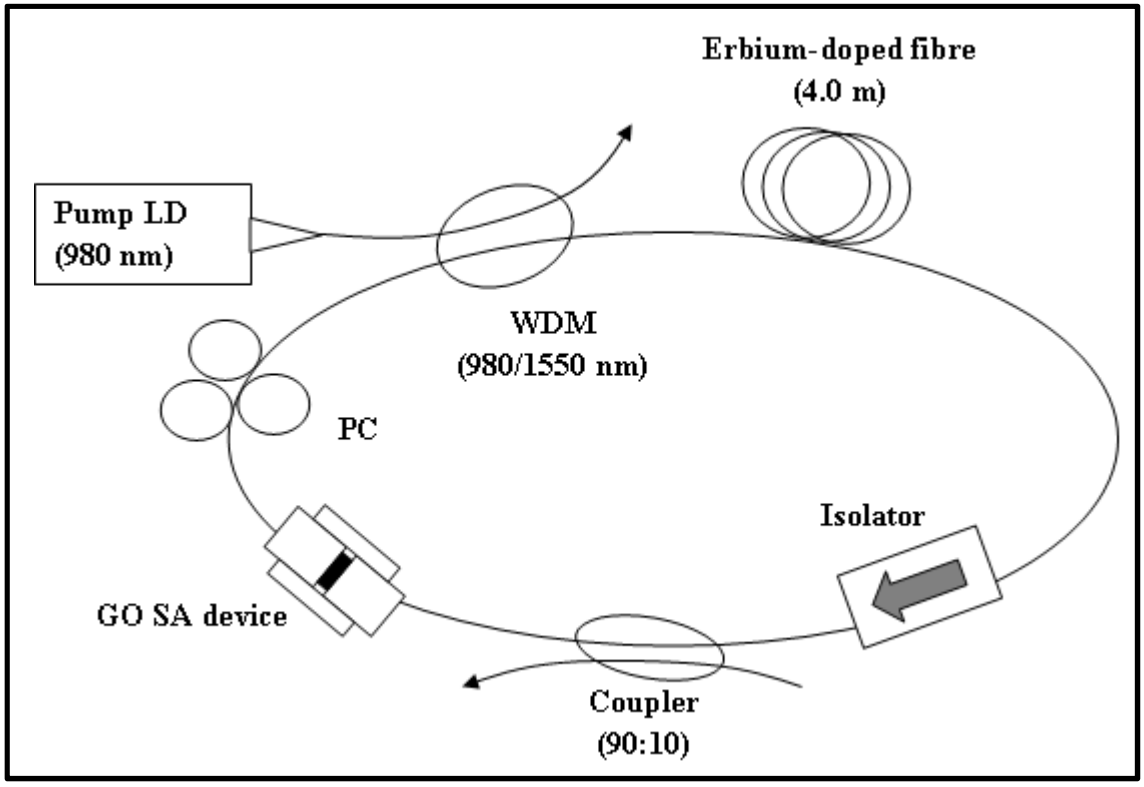

Figure 5.1: GO-based erbium-doped fibre laser (EDFL) ring configuration.

To make a GO based SA, 'dip-coating' method is employed (Figure 5.2), where the fibre ferrule is gently placed into the GO solution, and the GO suspension will stick to the fibre end surface accordingly, due to considerable adhesive force. The fibre ferrule was then allowed to dry at room temperature for 1 hour. After that, the ferrule is connected to another fibre pigtail via a FC/PC fibre adapter.

This way of transferring GO onto a fibre ferrule end to prepare a GO-based SA is demonstrated the first time. Compared to the method in [1], the method used here has the most exciting advantages of being simple, direct and efficient, without involving tedious and long experimental procedures and time. Massive scalability is possible. The GO suspension is readily available on the fibre ferrule for connecting it with another fibre pigtail via a connector (FC/PC) to make it a simple SA device, suitable for use in *Q*-switching and mode-locking of fibre lasers. Further comparison with that in [2], this method is cost effective – it does not require costly setup and complicated tunable optical parameters. Besides that, the fibre ferrule does not have the risk of being damaged by high intensity light in the core. By further controlling the concentration of the suspension during the GO synthesis process, it is believed this method is a promising candidate for low-cost and simple fabrication of graphitic material based SA device in an all-fibre format.

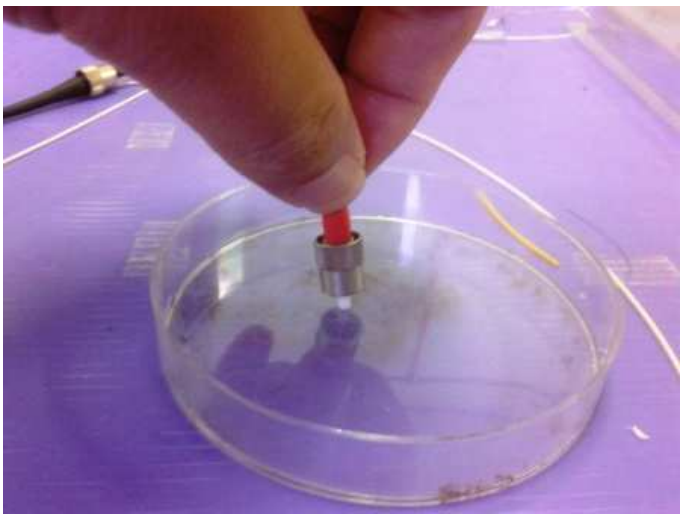

Figure 5.2: A GO based device was made by gently dipping a fibre ferrule end face onto the GO suspension.

5.1.1 Results and Discussions

The lasing oscillation of typical continuous wave (CW) operation pump threshold is about 4.8 mW. When the pump power is over 9.5 mW, the laser exhibits *Q*-switched operation.

Figure 5.3 shows the CW (without the graphene oxide) and *Q*-switched (with the graphene oxide) operation of the average output power as a function of incident pump power. At maximum pump power (84.0 mW), the maximum output power of the CW and *Q*-switched laser is 3.2 mW and 2.8 mW, respectively. The lower slope efficiency compared with the one at CW operation is due to the increased intracavity losses caused by the added GO for *Q*-switching. The ratio of the output power between GO pulsed and CW operation has a value of approximately 0.88, indicating a low insertion loss of the GO flakes, having great potential to be used as a novel saturable absorption device.

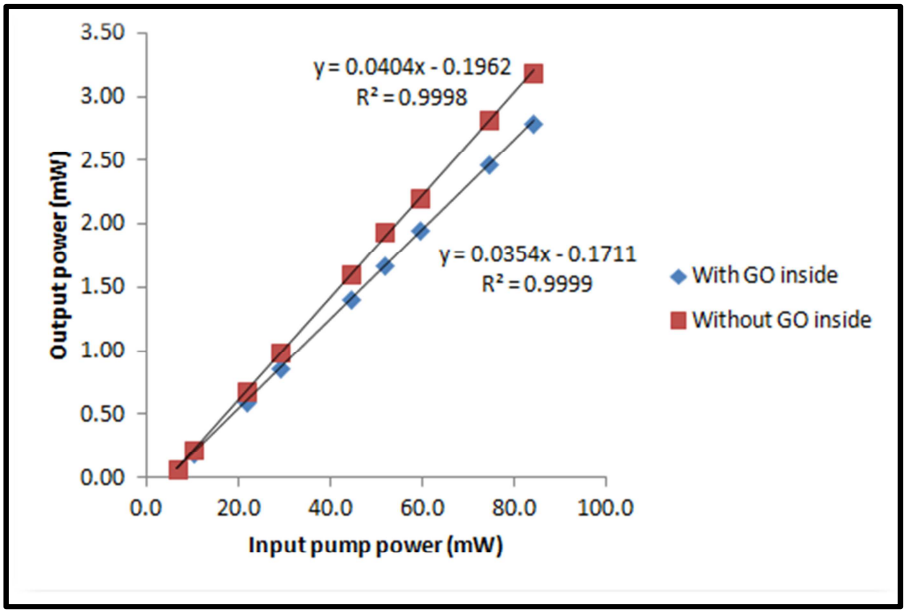

Figure 5.3: Output power as a function of input power at 1558 nm.

The CW and *Q*-switched pulse spectrum is measured and investigated by an optical spectrum analyzer (Anritsu MS9780A). The spectrum for both CW and pulse operation is shown in Figure 5.4. The central wavelength is 1558 nm. The spectral width at full-width-half-maximum (FWHM) of the pulsed operation is 3.12 nm.

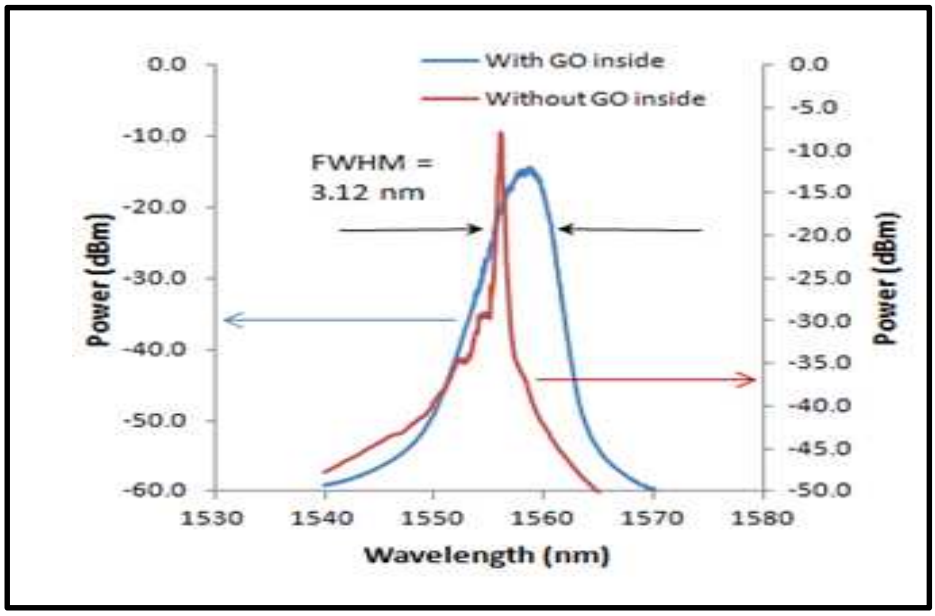

Figure 5.4: Typical laser spectrum of a EDFL, with and without the GO device inside the cavity.

To study the characteristics of the *Q*-switched pulses, the variation of repetition rate and pulse width by only manipulating the pump power is observed. Figure 5.5 shows the relationship between the pulse repetition rate and pulse width with the pump power. The repetition rate varies from 16.0 kHz to 57.0 kHz, with a rate of 22.7 kHz for a 13.6 mW pump power. In mode-locked lasers, the cavity length determines the repetition rate [3]. This is not so in the case of *Q*-switched lasers, where the repetition rate is very much dependent on the pump power [3]. When the pump power is increased, more gain is available to cause saturation to the SA. As pulse generation relies on saturation, the repetition rate would have a linear relationship with the pump power i.e the repetition rate increases with pump power [3]. The pulse width decreases with increasing pump power, which is consistent with the findings of [4]. It is shown here that the pulse width can be significantly narrowed down from about 24.0 μs to about 3.90 μs by changing

the pump power from ~10.0 mW to ~70.0 mW. It is believed that the pulse width could be further reduced by having a shorter length of the laser cavity design and optimizing the cavity loss [5, 6]. Figure 5.6 shows the typical pulse train and single pulse trace at an approximate pump power of 13.6 mW.

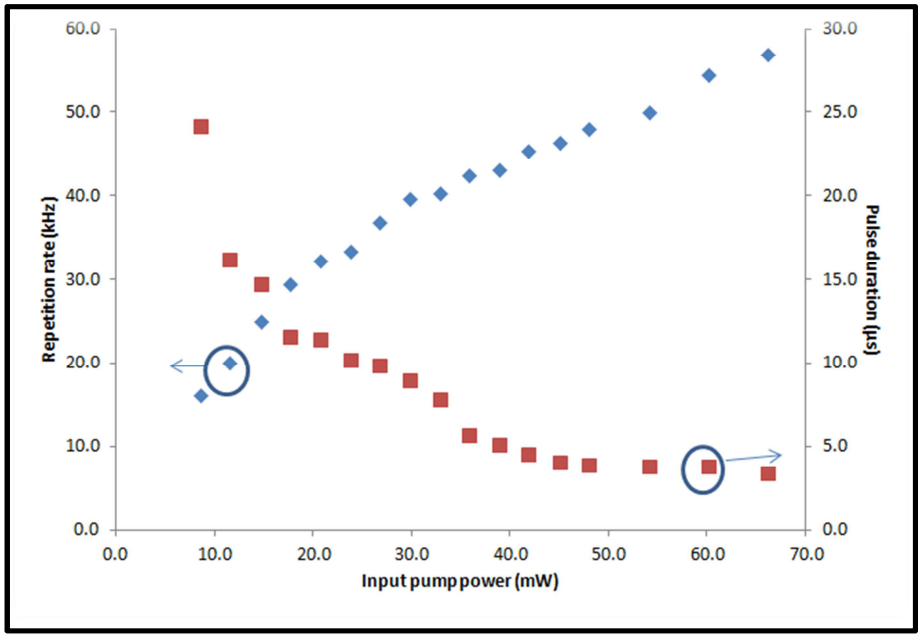

Figure 5.5: Pulse width and repetition rate as a function of the incident pump power.

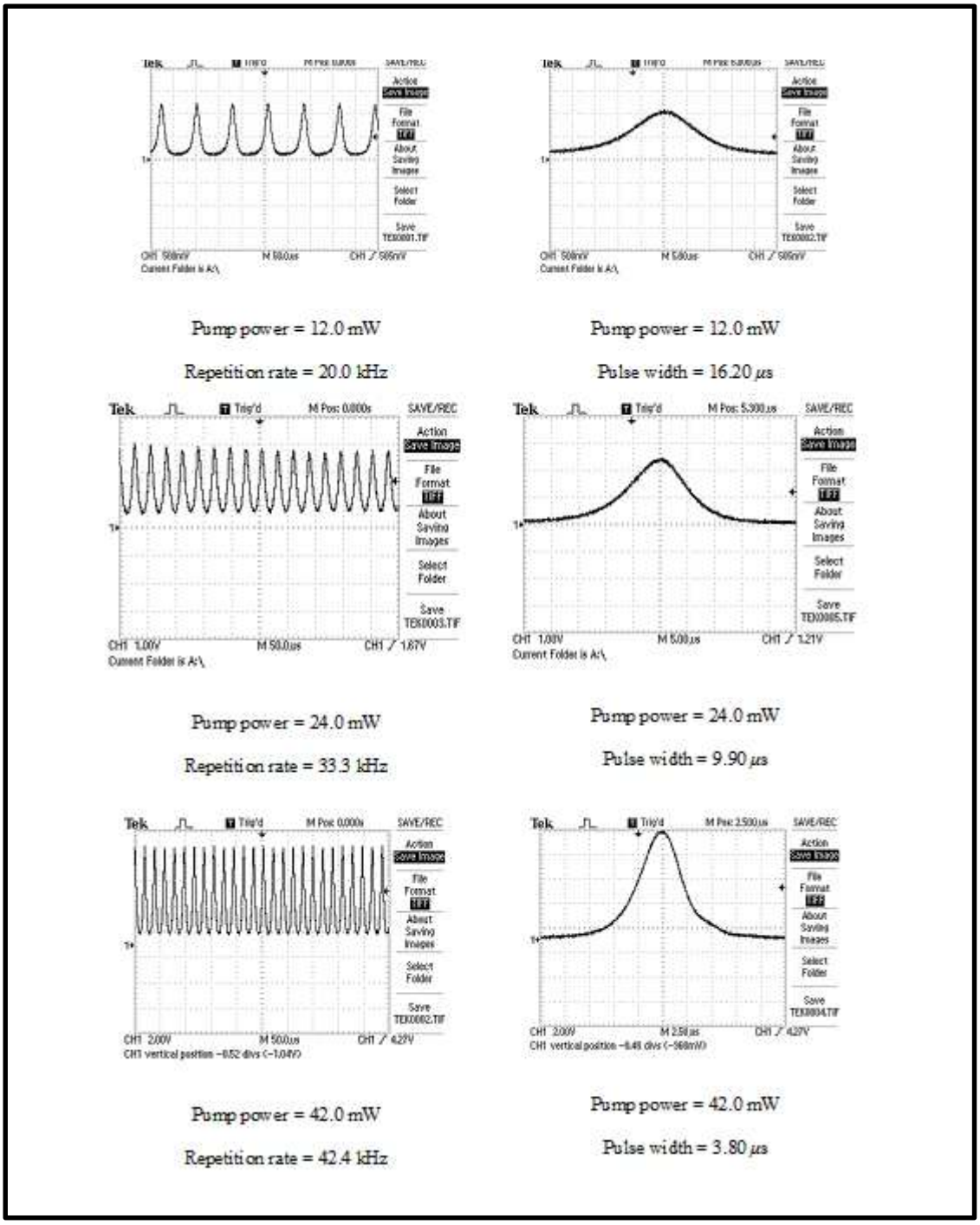

Figure 5.6: Typical oscilloscope traces of *Q*-switched pulse train (left) and extended single pulse shape (right), showing the pulse repetition rate and pulse width respectively under different pump powers.

The single pulse energy, E, can be calculated using the expression

$$E = \frac{P_{out}}{\nu} \quad \ldots\ldots (5.1)$$

where P_{out} is the average output power and ν is the pulse repetition rate. Figure 5.7 depicts the dependence of single pulse energy against pump power. As it is shown, the single pulse energy increases monotonously along with the pump power. The largest pulse energy of 38.2 nJ is obtained at the pump power of about 66.0 mW. It is clear that the single pulse energy is linearly dependent on the pump power. The energy varies from 8.3 nJ to approximately 38.0 nJ, corresponding to the range of pump power from ~ 10.0 mW to ~ 70.0 mW. Larger pulse energy could be enabled by increasing the pump power, using high gain fibre for large energy storage [7] and optimizing the coupling output and cavity loss [5].

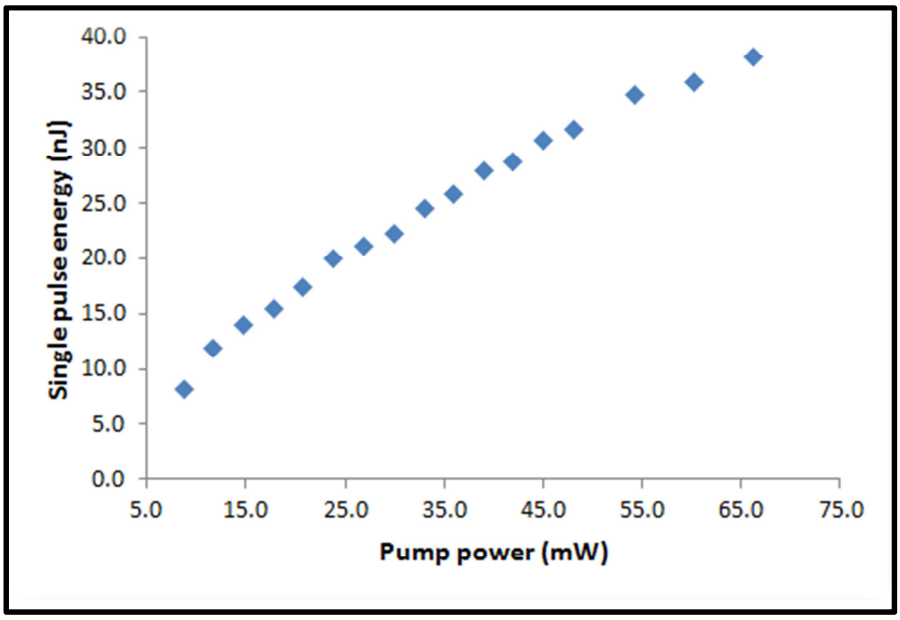

Figure 5.7: Single pulse energy as a function of pump power.

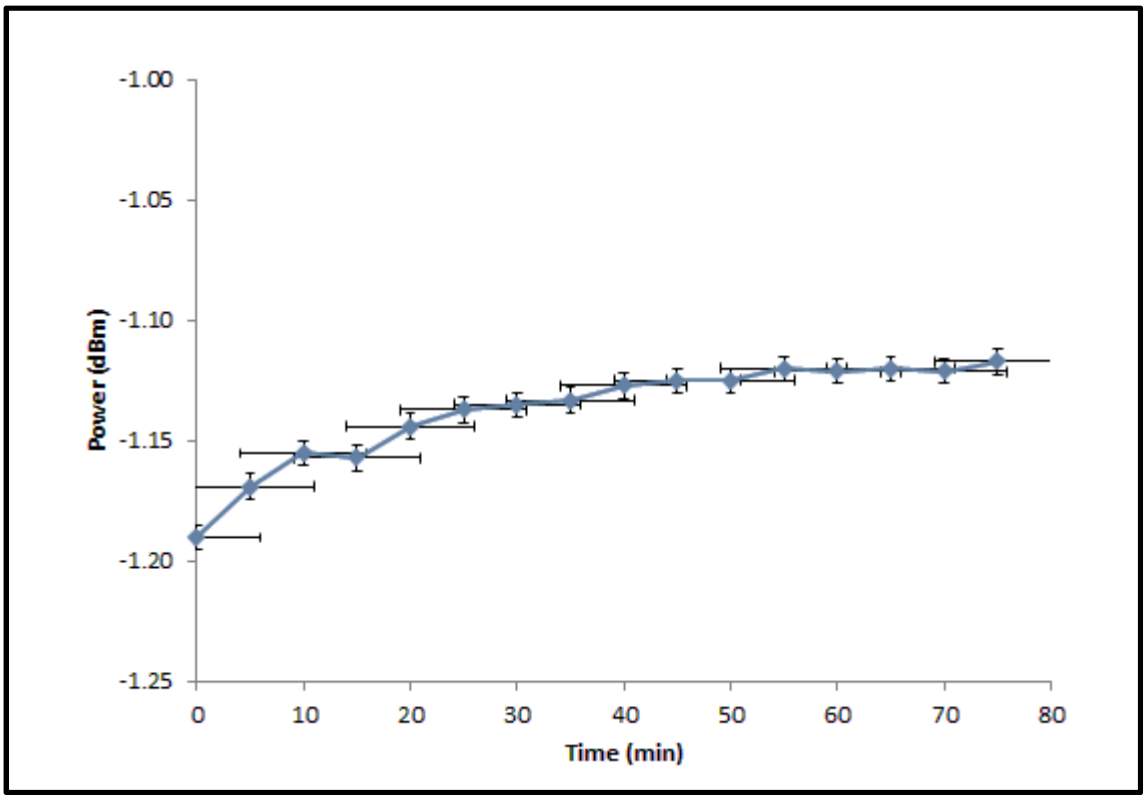

Figure 5.8: Fluctuation of average power of the *Q*-switched pulse.

Figure 5.8 shows the *Q*-switched pulse power fluctuation. It can be seen that the average output pulse power experienced some increase against the observation time. The slight increment could be due to temperature fluctuation of the laser diode used in the experiment overtime. The diode is not thermoelectrically cooled (cooler-less). Henceforth, small temperature fluctuation in the pump laser is inevitable, causing slight changes in the pump power, though the monitoring process was carried out at a constant driving current. Nonetheless, the overall power fluctuation of about 0.1 dB, corresponding to less than 3% in about 70 minutes, is within the measurement error and accuracy of the optical power meter used, indicating a good short-term stability of the pulsed laser output.

5.2 Graphene Oxide 'Paper'-based *Q*-switched Fibre Laser

Free-standing paper-like or foil-like materials are an integral part of science and technology applications. Inorganic 'paper-like' materials based on nanoscale components have been intensively studied [8, 9] and commercialized. Carbon-based flexible graphite foils [10-12] composed of stacked platelets of expanded graphite have been in use. The discovery of carbon nanotubes brought about bucky paper [13] which displays excellent mechanical and electrical properties that make it potentially suitable for fuel cell and structural composite applications [14-17].

In this section, the preparation of GO paper, a free-standing carbon based membrane material made by flow-directed assembly of individual GO sheets. This new material outperforms many other paper-like materials in stiffness and strength. Its combination of macroscopic flexibility and stiffness is a result of a unique interlocking-tile arrangement of the nanoscale GO sheets.

Most of the works emphasize on the use of GO sheets or flakes to fabricate a passive SA device. It has been shown that GO sheets can be assembled into a paper-like material under a directional flow – forming GO 'paper', where the GO sheets are orderly stacked [18].

GO paper is fabricated by filtration of the GO solution using a filter paper. The purpose of the filter paper here is to ensure a directional flow of the solution where the GO sheets can be assembled into a well-ordered structured. 10 ml of the solution was filtered, after which it was left to dry at room temperature for a day. Figure 5.9 shows the as prepared GO paper.

Figure 5.9: Image of the GO ‘paper’ obtained through filtration.

5.2.1 Results and Discussion

5.2.1.1 Characterization of GO 'Paper'

Figure 5.10 shows a close-up examination of the GO using a Field Emission Scanning Electron Microscope (FESEM – JSM 7600 F). After filtration, it shows an orderly layered GO sheets, verifying the formation of GO paper [18].

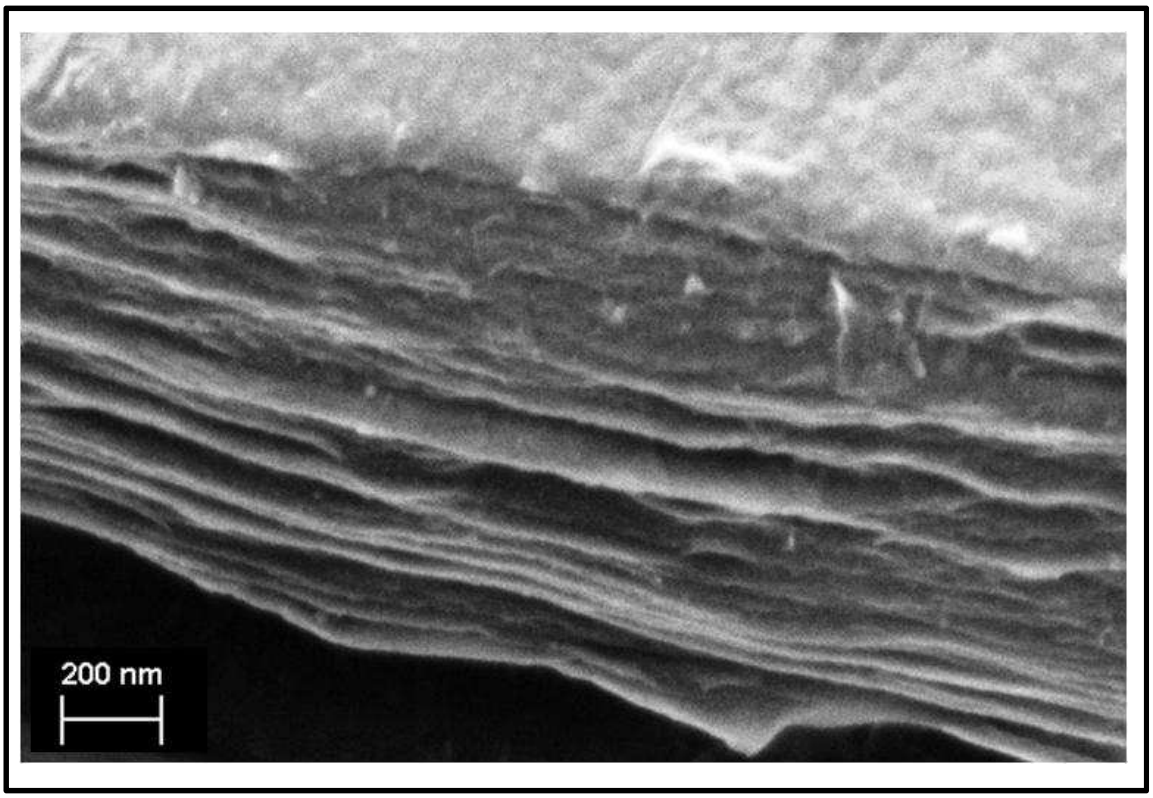

Figure 5.10: Orderly stacking of GO layers, indicating the formation of GO 'paper'.

Also, from the X-ray diffraction (XRD) results as discussed in the previous chapter, the peak of 8.9^{o} in the spectrum of a typical GO paper corresponds to a layer to layer of distance (*d*-spacing) of about 1 nm, using Bragg's Law of XRD, indicating the presence of a large number of water molecules intercalated in the GO sheets, as reported by [19] and [20]. The measured distance could be attributed to an approximately one molecule thick layer of water that is presumably hydrogen-bonded between the GO sheets. Since GO itself is an allotrope of carbon whose structure is one-atom-thick planar sheets of sp^2-bonded carbon atoms, which has nano-scale dimensions, the measured dimension of

the orderly stacked GO sheets that assemble a paper material can be calculated using Debye-Sherrer equation, given by

$$\tau = \frac{K\lambda}{\beta \cos\theta} \quad \text{..... (5.2)}$$

where τ is the average size of the crystalline domains, K is the shape factor, β is the line broadening at full wave half maximum intensity of the X-ray diffraction peak and θ is the Bragg's angle. Assuming a crystallite structure of graphite and taking K to be 0.89, the mean dimension of the GO paper was found to be about 6.5 nm, which corresponds to about 6 to 7 stacked GO sheets.

5.2.1.2 *Q*-switched Erbium-doped Fibre Laser using GO 'Paper'

The SA device is fabricated by cutting a small part of the prepared GO paper (2 × 2 mm^2) and sandwiching it in between two FC/PC fibre adapters, after. The insertion loss of the SA is measured to be around 3.5 dB at 1550 nm. The insertion loss could be reduced by diluting the GO solution before pouring it to the Petri dish for film formation. The SA is then integrated in a EDFL setup, same as that shown in Figure 5.1. The pulse threshold of the proposed system is found to be approximately 68 mW, with the pump power of the system being limited to 150 mW, which is the maximum output level of the LD. The optical spectrum of the *Q*-switched pulses generated by the system is shown in Figure 5.11.

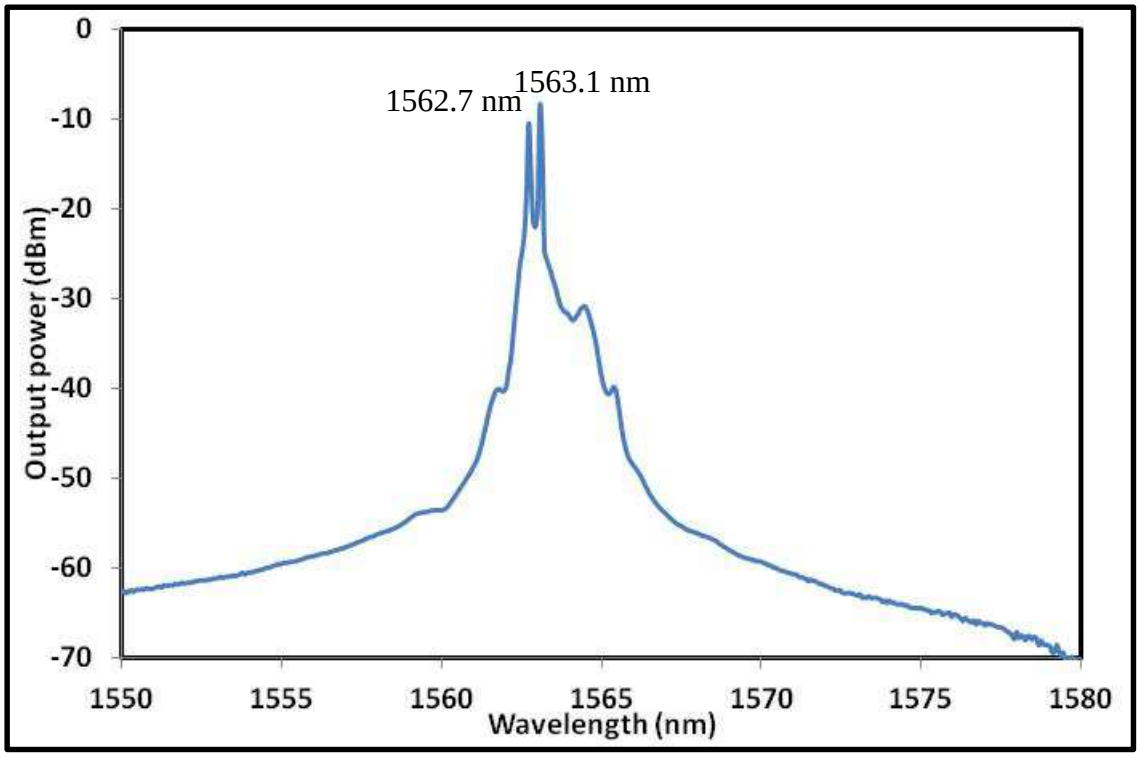

Figure 5.11: Optical spectrum of the *Q*-switched laser at 150 mW.

It can be seen from the figure that there are two distinct peaks present, at 1562.7 nm and 1563.1 nm. The centre wavelength of the spectrum is approximately 1563.1 nm, with a broad spectral width. This is expected of a *Q*-switched laser pulse.

Figure 5.12 shows the evolution of the output optical spectrum as the pump power is increased from 98 mW to 150 mW.

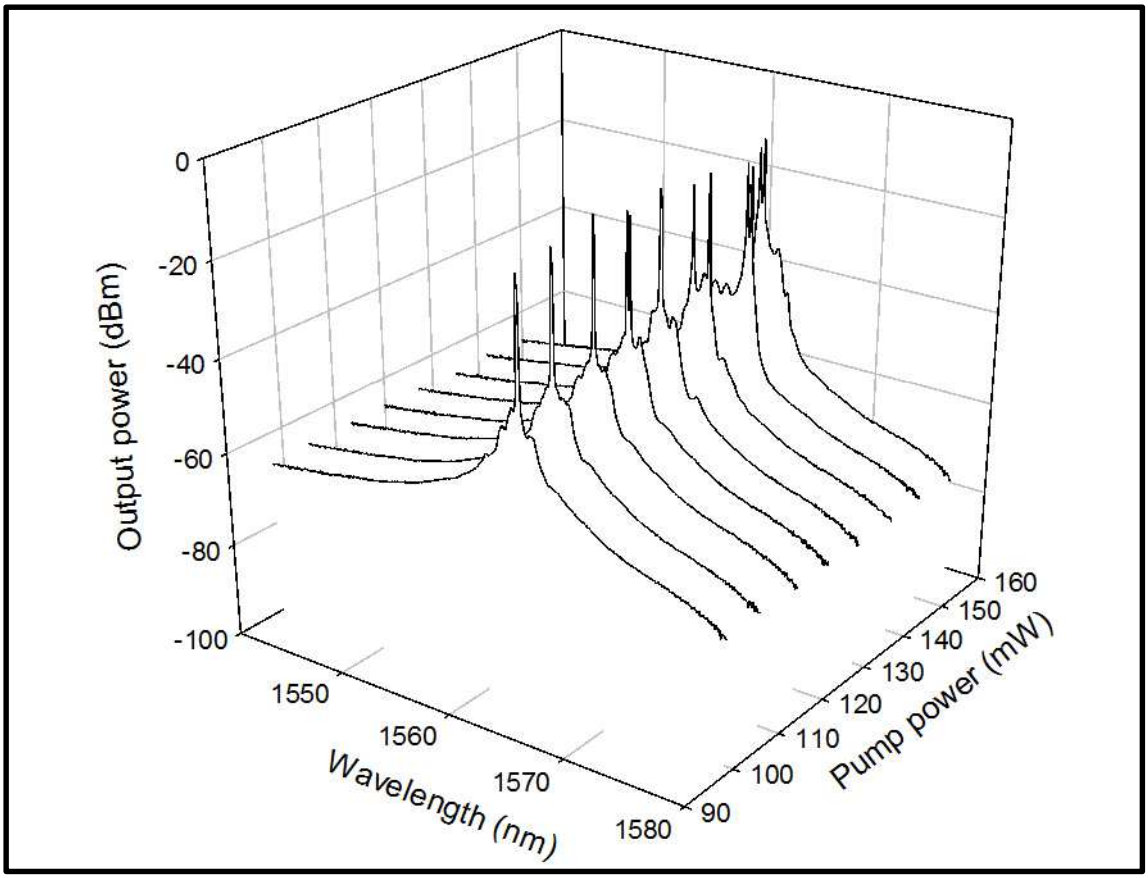

Figure 5.12: Evolution of optical spectrum for pump power varied from 98 to 150 mW.

Figure 5.13 (a) and (b) show the pulse train and single pulse envelope obtained at a pump power level of 150 mW. The pulse train is observed to have a repetition rate of 21.5 kHz with a pulse-to-pulse spacing of about 46.5 μs. The individual pulse width is about 3.8 μs, taken at the full-width at half-maximum (FWHM) of the single pulse envelop

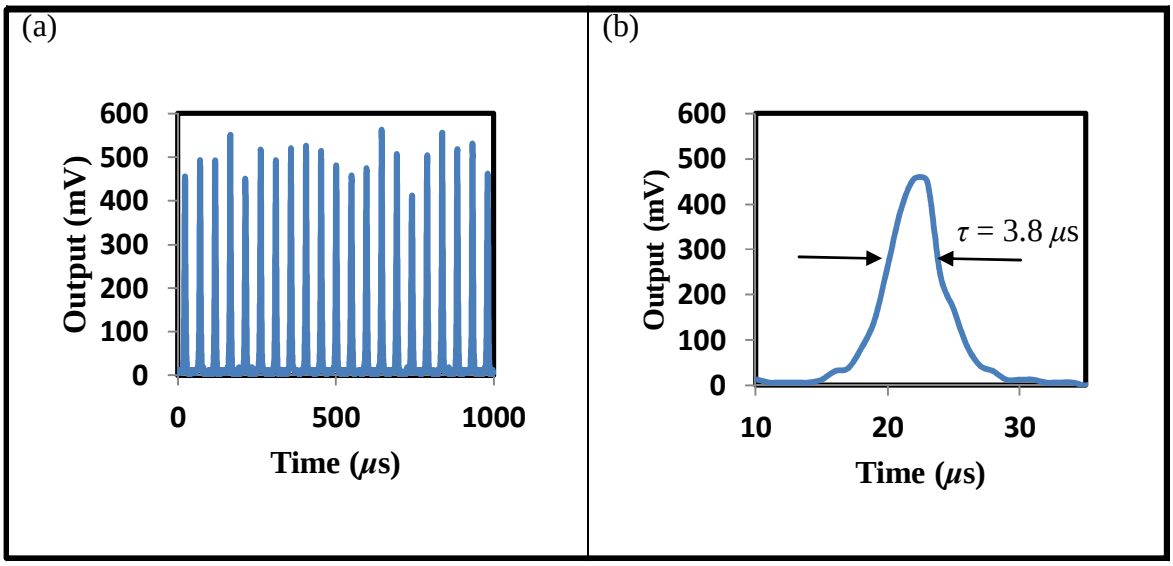

Figure 5.13: (a) Pulse train and (b) single pulse envelope at a pump power of 150 mW.

In order to fully characterize the performance of the GO paper-based SA, the pump power of the pulse system is varied from the minimum to the maximum, covering a range from 68 mW, which is the pulsing threshold, to 150 mW, which is the maximum pump power available in this experiment. Figure 5.14 shows the pulse width and pulse energy of the system as a function of different pump power levels.

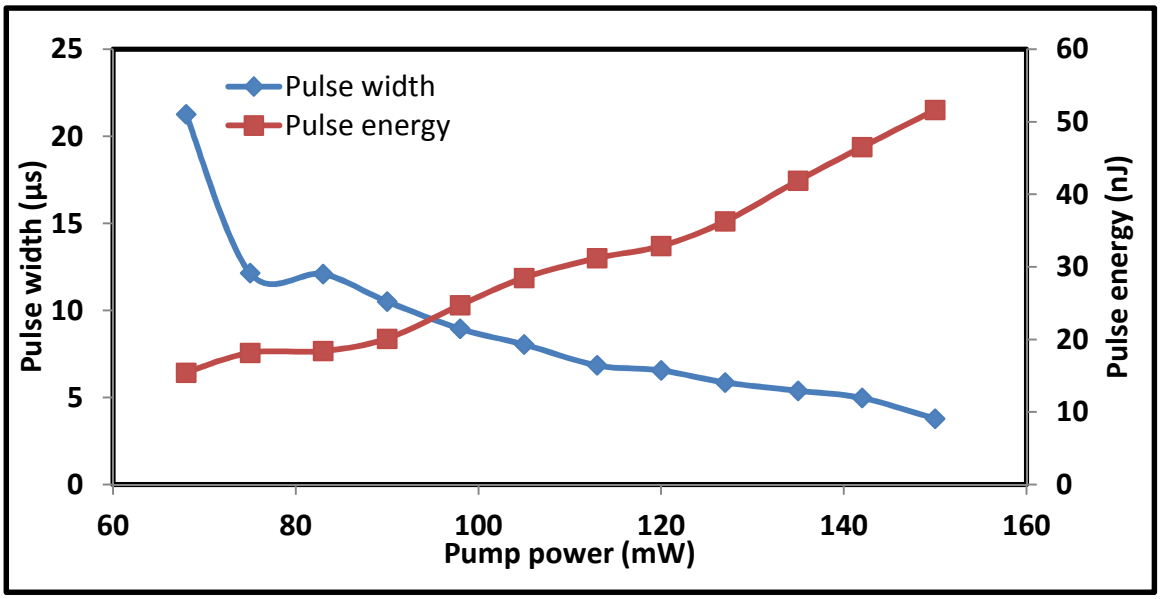

Figure 5.14: Pulse width and pulse energy of the *Q*-switched laser as a function of different pump power levels.

From Figure 13, it can be seen that the pulse width decreases rapidly as the pump power increases over the range from 68 to 78 mW, dropping from a maximum value of 21.3 μs to approximately 12.1 μs. This gives an initially gradient of about -1.0 μs/mW, Subsequent increase in the pump power, on the other hand, does not lead to such a significant drop in the pulse width, with the lowest pulse width obtained being 3.8 μs at a pump power of 150 mW – which gives a much smaller gradient, of about only - 0.1 μs/mW linearly, or about 10% of the initial gradient. A similar, though inverse relationship, is observed for the case of the pulse energy plotted against the pump power, with two gradient regions, one at the initial stage and another covering the remainder of the graph. At the initial stage, the minor increase in the pump power resulted in substantial increase in the pulse energy, with the pulse energy jumping from 15.4 nJ, at a pump power level of 68 mW, to 20.1 nJ, at a pump power level of 90 mW. Subsequent increase in the pump power level however results in less substantial increase in the pulse energy, with the pulse energy increasing to 51.7 nJ at the maximum pump power level of 150 mW. This gives two separate, almost linear gradients – with the initially gradient being about 0.2 nJ/mW and the following, steeper gradient being about 0.5 nJ/mW. This behaviour is similar to that of the pulse width. The maximum pulse energy generated by this setup is higher than that observed in the similar setup demonstrated in Section 5.1.1, although obtained at a higher pump power level.

The repetition rate of the pulses generated by the system, as well as the average output power of the system, increases at a linear rate with the pump power – as would be expected from a *Q*-switched system. The repetition rate varies from 15.6 kHz to 21.5 kHz from a pump power level increasing from 68 mW to 150 mW, giving a linear relationship with a gradient of about 0.1 kHz/mW. The average output power also increases in a similar manner, from 0.2 mW to 1.1 mW for a pump power range of 68 to

150 mW. The gradient obtained for this linear relationship is about 0.01 kHz/mW. Figure 5.15 shows such changes in the repetition rate and average output power as described when the pump power is increased.

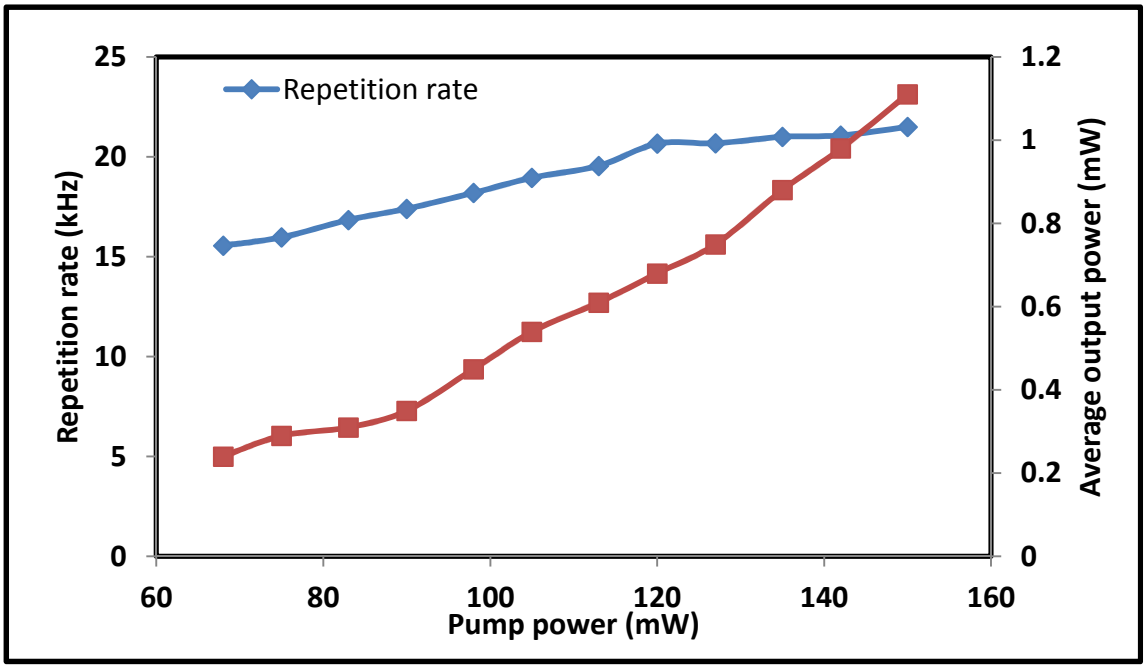

Figure 5.15: Repetition rate and average output power as a function of pump power.

5.3 Reduced Graphene Oxide-based *Q*-switched Fibre Laser

One of the most interesting features of GO is that it can be partially reduced to graphene-like sheets by removing the oxygen-containing groups. Hence, functionalized graphene, or more commonly known as reduced graphene oxide (rGO), can be realized. rGO cannot be considered as pristine graphene because the remaining functional groups greatly change the structure of the carbon plane and the properties are significantly different.

Since rGO is chemically derived graphene, rGO has saturable absorption property as well. In view of this, a rGO-based EDFL is proposed and the GO-based EDFL in Section 5.0 is compared with this rGO-based EDFL. In this section, commercially available graphene flakes (rGO) in N-Methyl-2-pyrrolidone (NMP) solution from *Graphene Research* was characterized by UV-Visible spectroscopy and Raman spectroscopy. The rGO was transferred onto a fibre ferrule using 'dip-coating' method as described in Section 5.0 to fabricate a passive SA device. The rGO-on-ferrule device is then allowed to dry in air at room temperature before it could be ready to be used as a SA device.

Before the SA device is used, the rGO is first measured its linear absorption using a *Perkin-Elmer 1050 UV-VIS-NIR spectrophotometer*. *Renishaw inVia Raman Microscope* is used to perform Raman measurements on rGO flakes drop-casted on glass substrate, at 514 nm wavelength excitation. All measurements are carried out at room temperature. For *Q*-switched EDFL demonstration, the rGO device is 'sandwiched' between two fibre adapters and incorporated into the ring laser resonator as shown in Figure 5.1.

5.3.1 Results and Discussions

5.3.1.1 Characterization of Reduced Graphene Oxide

Figure 5.15 shows the UV to visible absorption spectrum of the rGO flakes. The most important features of the spectrum are the ultraviolet peak at 256 nm, which corresponds to the $\pi \rightarrow \pi^*$ transition of aromatic *C-C* bonds - and a shoulder at 284 *nm* that can be assigned to the $n \rightarrow \pi^*$ transition of *C=O* bonds, known as carbonyl groups [21, 22]. The maximum absorption peak appears between 250 - 270 nm, which is the range observed in rGO material [23]. In the visible region (400 - 700 nm) the absorption spectrum is almost flat with a very low absorption, which is in agreement with the theoretical explanation that graphene material absorption in the visible range is wavelength independent [24]. The low absorption in this range indicates that there are few remaining flakes in the solution used. At wavelengths lower than 250 nm a considerable amount of fluctuation is observed. This fluctuation could be the result of variations in the baseline measurement obtained from NMP solution, since it has no effect on the performance of the device – because, after optical deposition, there is no NMP remaining on the ferrule.

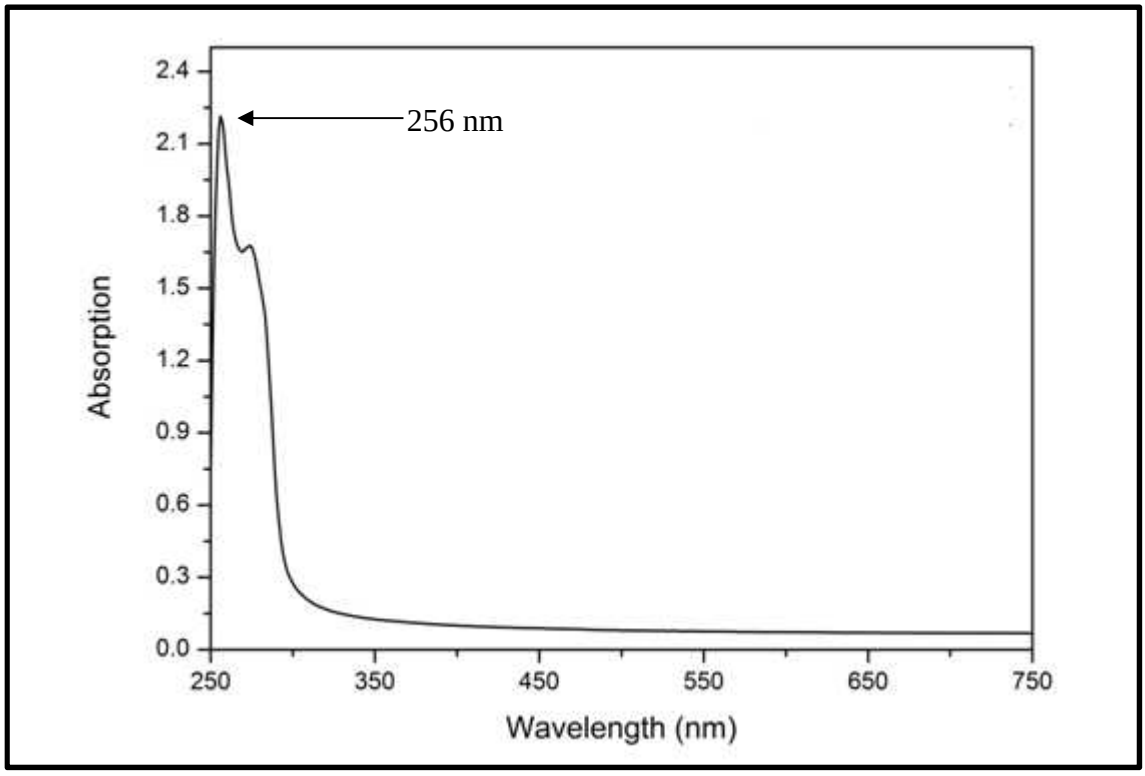

Figure 5.16: UV to visible wavelength absorption spectrum of rGO flakes dispersed in NMP solution.

The Raman spectrum of the rGO is shown in Figure 5.17, similar to that of [25]. The *D* peak at about 1350 cm^{-1} originates from the breathing modes of phonons and requires the presence of defects for its activation by double resonance [26-28]. It provides information on defects and disorder in the system. The high intensity of the *D* peak suggests the presence of a number of defects in the sample. On the other hand, due to the doubly generated E_{2g} peak at the Brillouin zone center and in-plane vibration of sp^2 atoms, the *G* peak is found to be at 1582.3 cm^{-1} [29]. Furthermore, the ratio of the peak intensities, I_d/I_g, is a measure of the disorder of the crystalline graphene [23, 28]. For the measured sample, I_d/I_g is 0.895 which could originate from structural defects and vacancies.

The peak at 2715.28 cm^{-1} is called the 2*D* band - the second order of the *D* peak. It is produced by the second order zone-boundary phonons [30]. The 2D band provides information on the stacking order of layers in sample: for instance in single layer

graphene material, this peak is a single band, while it splits into four sub-bands in bilayer graphene material or appears with multiple peaks in multilayer materials, which is also a demonstration of the dependence of 2*D* band on the number of layers and the splitting of the electronic band structure in multilayer material [29, 31].

In the Raman spectrum obtained, the low intensity, broadening and up-shifting of the 2*D* band are an indication of a multilayer structure. As the number of layers increases, the intensity of the *G* band rises and the 2*D* band becomes progressively more blue-shifted. Unlike the *D* band, the 2*D* peak is always seen in the spectrum as it originates by activation of two phonons with the same momentum, but opposite wave-vector, and no defects are required for the process to occur [30-32]. The second order zone-boundary phonons do not satisfy Raman selection rules - and therefore they cannot be observed in the first order Raman spectra of defect-free samples [30]. However, the second order peak of the 2*D* band always appears in the Raman spectrum.

The *D* + *D*' band (at 2942 cm^{-1}) is also the result of two phonon excitation but of opposite momentum around *K* and *Γ* and requires defects for its activation [31].

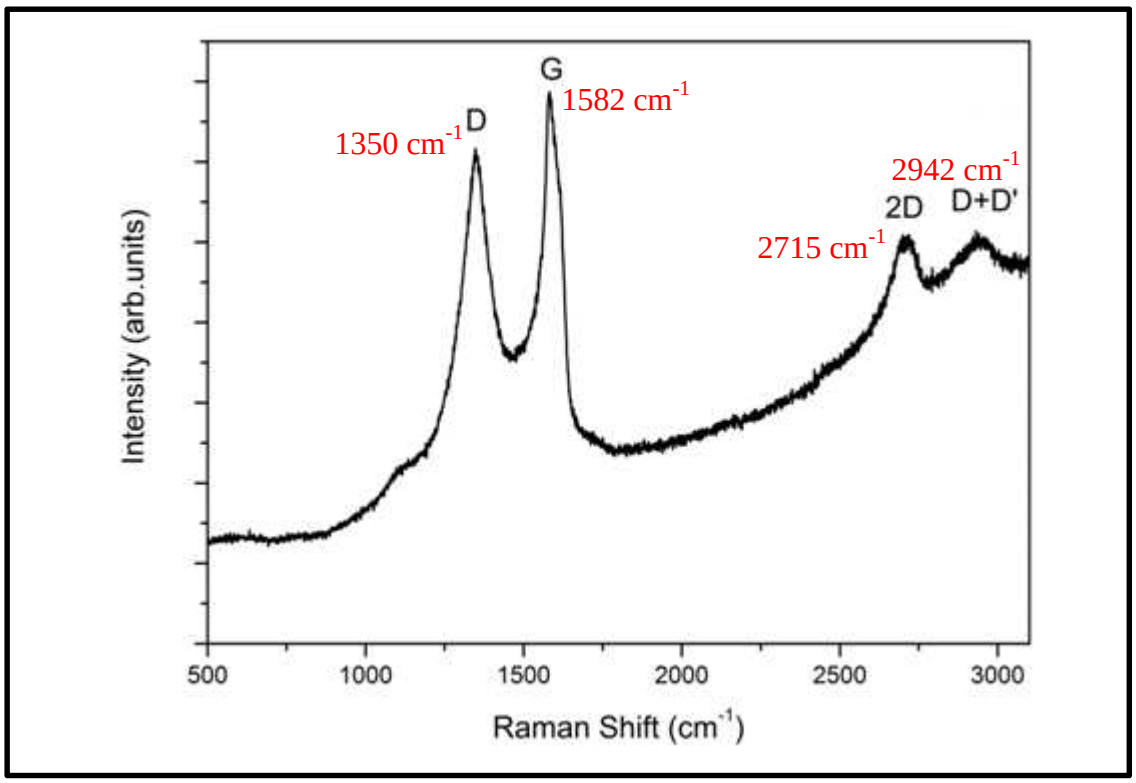

Figure 5.17: Raman spectrum of rGO flakes deposited on a glass substrate.

5.3.1.2 *Q*-switched Erbium-doped Fibre Laser using Reduced Graphene Oxide

By increasing the diode power, continuous wave (CW) operation starts at a pump power of 2.8 mW. With careful adjustment on the PC, pulsing begins at a pump power of about 10.5 mW. This threshold for *Q*-switched pulse operation is much lower than some previous work on graphene materials *Q*-switched fibre lasers [33-38]. Figure 5.18 shows the dependence of the average output power on the incident pump power, with and without the rGO device inserted into the ring resonator. The output power increases with the pump power, with rGO inside the cavity, as shown in Figure 5.18. Under the incident pump power of 84.2 mW, the average output power was about 2.18 mW, corresponding to a slope efficiency of 2.7%. The efficiency of the laser is a few times better than that of [39]. To ensure that the pulses are caused by the saturable absorption of rGO, we purposely removed the rGO-on-ferrule device from the resonator. No pulses were observed under available maximum pump power. The maximum output power was approximately 2.4 mW under the maximum pump power of 84.2 mW, giving a slope efficiency of 2.9%, slightly higher than that under pulsed operation by a factor of

about 7%. The output power ratio between rGO pulsed laser and CW operation has a value as high as 0.91. Such results show that rGO has insertion loss at a very low level, which is good as a potential viable saturable absorber. Figure 5.219 shows the laser spectrum of the pulsed laser. The 3-dB bandwidth of the spectrum is 1.24 nm, at the centre wavelength of 1533.12 nm.

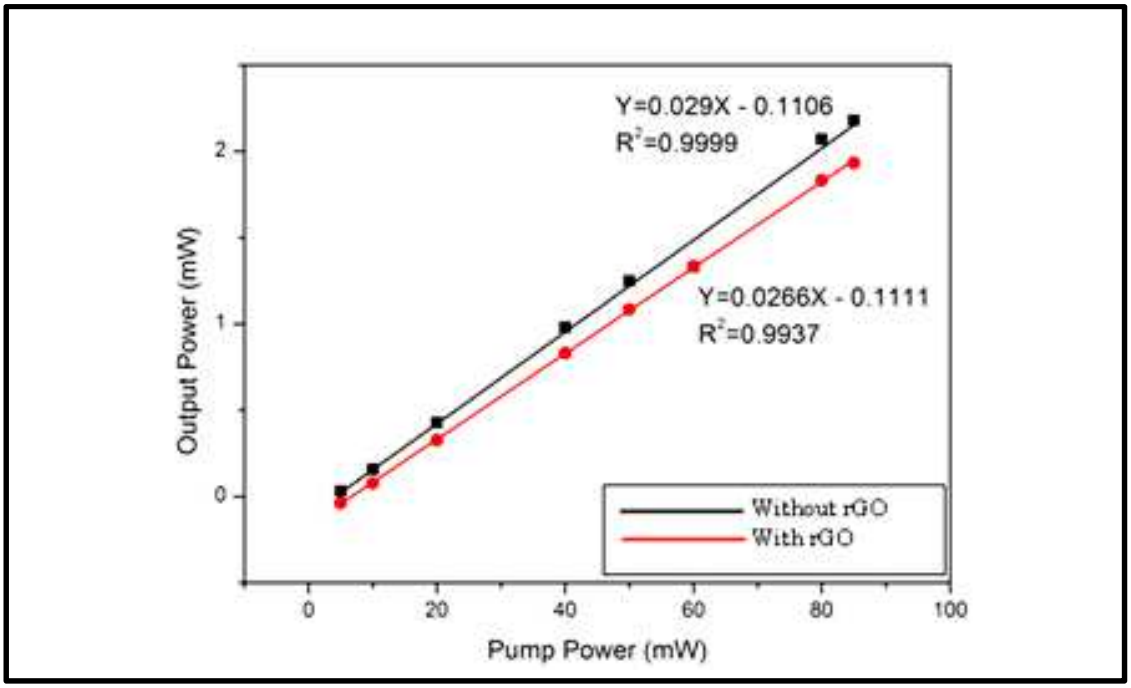

Figure 5.18: The laser output power as a function of diode pump power. The laser configuration with rGO inside has lower slope efficiency, indicating there is insertion loss caused by the material.

Correspondingly, the spectrum of *Q*-switched operation is shown in Figure 18. When the *Q*-switched operation was initiated, the spectrum exhibited the modulation structure due to the multimode oscillation and cavity perturbations [40].

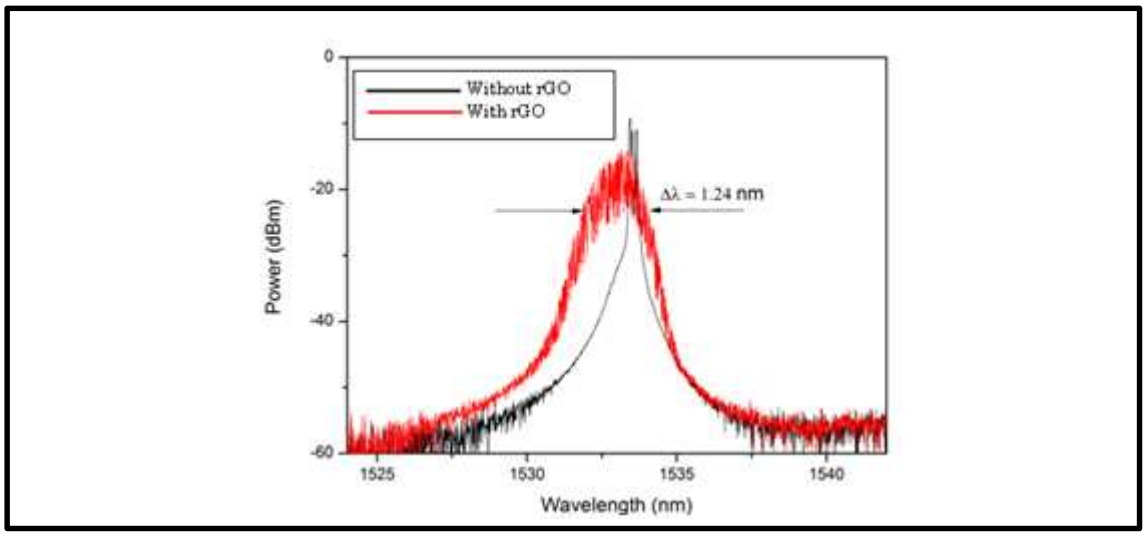

Figure 5.19: The laser spectrum of the rGO pulsed laser at centre wavelength of approximately 1533 nm.

Figure 5.20 shows the relationship of the pump power with the pulse repetition rate, in kilohertz range, which confirms the *Q*-switching operation of the ring laser. In *Q*-switching, the lasing is initially prevented by a low *Q* factor [3]. The stored energy is then released in a giant pulse followed by a high *Q* factor [3]. The time needed to replenish the extracted energy between two consecutive pulses is related to the lifetime of the laser gain medium, which is typically in the range of milliseconds in the case of EDF [3]. Thus *Q*-switched lasers usually have a lower repetition rate when compared to mode-locked lasers (~MHz) [3, 41]. In the *Q*-switched pulses shown here, the repetition rate can be tuned from ~21.0 kHz to ~70.0 kHz by varying the pump power from 15.0 mW up to 70.0 mW. Under the incident pump power of 60.0 mW, 58.1 kHz of repetition rate was achieved. In comparison, some previous work showed 28 kHz [28] and 45 kHz [35] under the same pump power of 70 mW. In short, the repetition rate is pump power dependent. This is true as the repetition rate relies on saturation [3][33]. The repetition rate can be further scaled up by increasing the pump power. In our case,

this is limited only by the available pump power. Figure 5.21 shows the *Q*-switched pulse train under the incident pump power of 25.9 mW and 40.9 mW respectively.

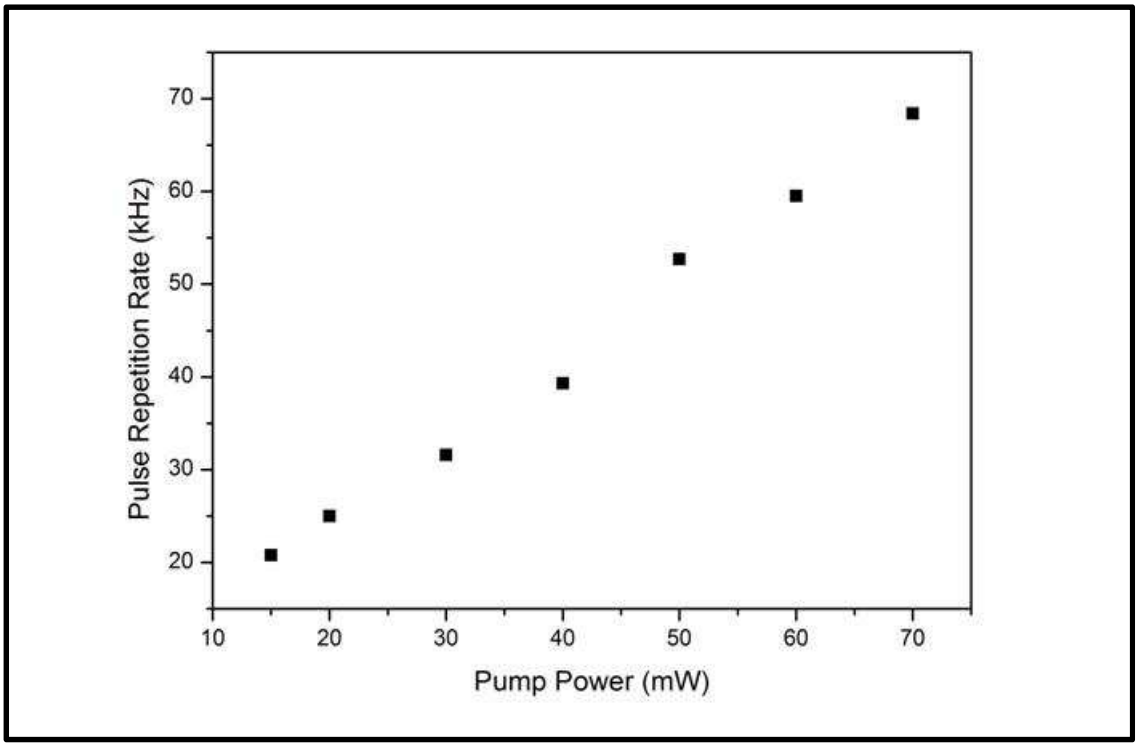

Figure 5.20: The relationship of the pulse repetition rate and the diode power. The repetition rate increases with increasing pump power, as at higher pump power, more gain is provided to saturate the rGO-based SA.

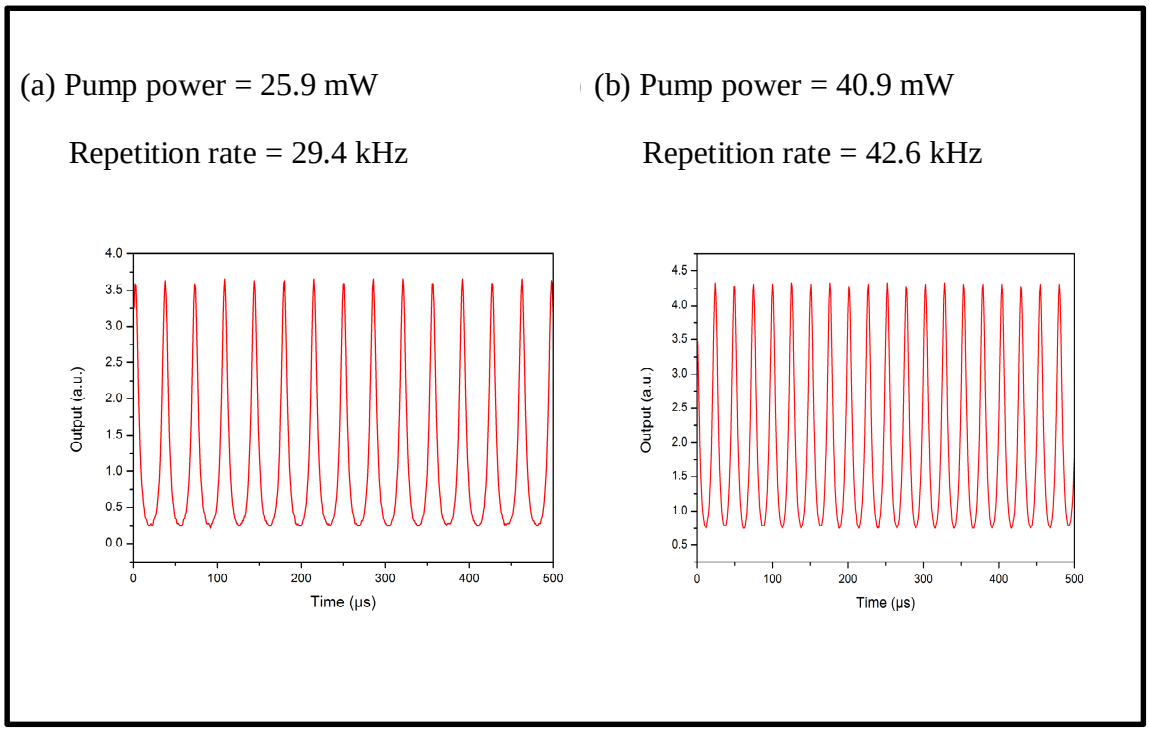

Figure 5.21: Typical pulse train of a *Q*-switched laser.

Figure 5.22 shows the relationship of the pulse width and the pump power. It shows clearly that the pulse width decreases with increasing pump power, which is consistent with the findings of [42]. It is shown here that the pulse width can be significantly narrowed down from ~12.0 μs to ~3.80 μs by changing the pump power from 15 mW to 50 mW. It is believed that the pulse width could be further reduced by having a shorter length of the laser cavity design and optimizing the cavity loss [5, 6]. Figure 5.23 shows pulse measurement at 16.2 mW and 40.9 mW respectively.

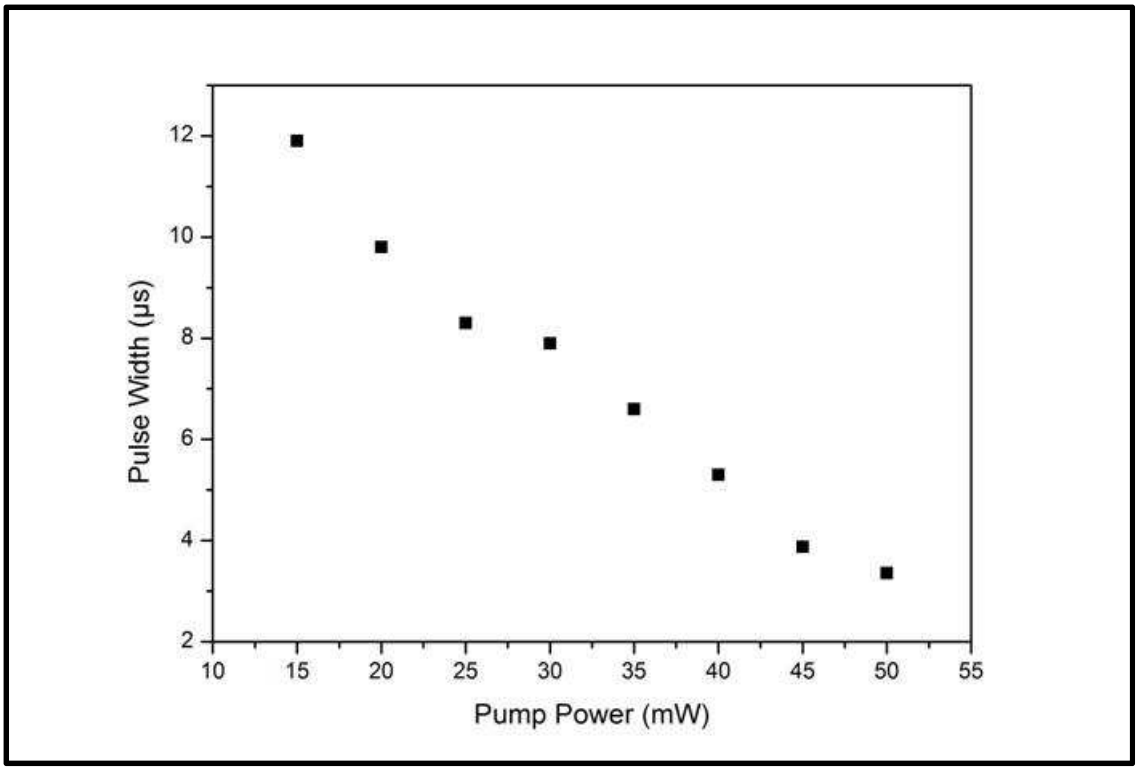

Figure 5.22: The pulse duration as a function of pump power.

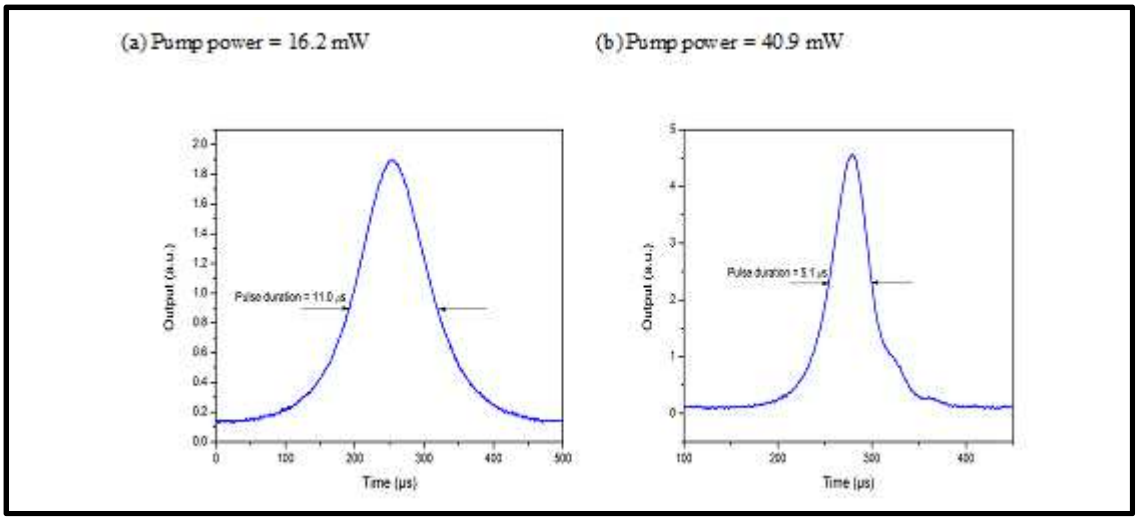

Figure 5.23: Single pulse trace under different pump powers.

On the pulse energy studies, the single pulse energy at 50.0 mW is calculated to be 24 nJ. Figure 5.24 shows the single pulse energy as a function of input pump power. It is shown here that the single pulse energy is linearly dependent on the pump power, with saturation at pump power exceeding 40.0 mW, which is consistent with that of [42]. The energy varies from 14 nJ to 26 nJ, corresponding to the range of pump power from 15

mW to 70 mW. Larger pulse energy could be enabled by increasing the pump power, using high gain fibre for large energy storage [43] and optimizing the coupling output and cavity loss [5]. In the case here, the pump power is not increased further, to protect the rGO from thermal damage.

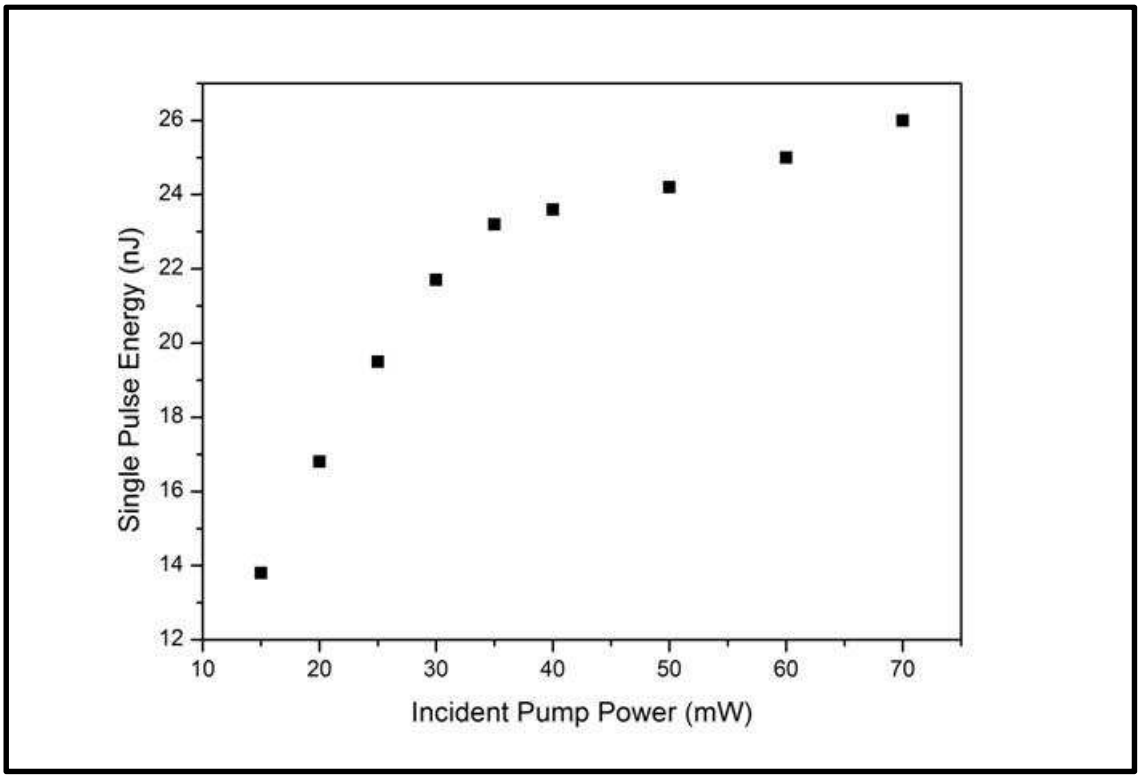

Figure 5.24: The calculated single pulse energy as a function of pump power.

5.4 Summary

The performance of the *Q*-switched fibre lasers here with GO coated on fibre ferrule by 'dip-coating', GO 'paper' and rGO can be compared objectively by observing a few laser parameters. The comparison between all achieved laser parameters is summarized in Table 5.1.

Table 5.1: Summary of the laser parameters with GO, GO 'paper' and rGO.

Parameter	**Value**		
	Graphene oxide 'dip-coated' on fibre ferrule	**Graphene oxide 'paper'**	**Reduce graphene oxide**
Centre Wavelength	1558 nm	1563 nm	1533 nm
Q-switched threshold	9.5 mW	68.0 mW	10.5 mW
Maximum output power	2.8 mW	1.1 mW	2.18 mW
Maximum repetition rate	57.0 kHz	21.5 kHz	70.0 kHz
Maximum pulse energy	81.0 nJ	51.7 nJ	26 nJ
Shortest pulse duration	3.9 μs	3.8 μs	3.8 μs

The main cause of the differences in the parameters could be the maximum pump power available. For GO 'dip-coated' on fibre ferrule, the pump power is not increased beyond 90 mW, as to protect the GO SA device from thermal damage. In the other hand, the GO 'paper' is anticipated to have a higher damage threshold, since it consists of 6 to 7 stacks of GO sheets as calculated from the XRD results in the previous section. This leads to a much higher *Q*-switching threshold. Therefore, higher pump power is required for saturation to occur since *Q*-switching relies on saturation, and this results in

lower values for most of the parameters. For the pulse repetition rate, rGO SA gives the highest value. rGO has much less functional groups compared to GO. Hence, it has a almost zero bandgap, resembling much the form of graphene. It is anticipated then rGO would saturate and recover faster. At the same level of pump power, the time to replenish the energy between two consecutive pulses is also much shorter and hence results in a higher repetition rate. It is believed that all the parameters can be scaled up with increasing pump power. Overall, there is almost no significant difference between the parameters achieved with both types of SA devices. The same pulse duration can be achieved for all three, under different pump powers respectively. Also, it can be said that the sp^3-hybridized carbons in the lattice does not completely destroy the nonlinear optical properties of GO. So it may not be necessary to perform a complicated reduction process just to fabricate a good pristine graphene SA.

5.5 Graphene Oxide-based Bismuth-based Erbium-doped Fibre Laser

In using silica glass host as a gain medium, EDFLs have received considerable attention. Most graphene materials-based *Q*-switched EDFLs used EDF as the laser gain medium [1, 4, 7, 25, 33, 35-39, 42]. For compact design of EDFL, short gain medium length is critical. To compensate for the short gain medium length, the active fibre needs to be doped with much higher erbium ion concentration. However, a high concentration erbium ion may result in a pair-induced quenching effect, which potentially reduces the pump power conversion efficiency and increase the noise figure of the laser [44-46]. Bismuth-based fibre has been intensively studied in the previous past for fibre laser applications [47-50]. This new non-silica based EDF was first reported by *Asahi Glass* Company. Bismuth-based fibre host has the ability to be highly doped with erbium. It possesses also a wideband emission spectrum, easy refractive index control and high reliability. Its wide absorption band makes it ready to be pumped by commercially available powerful laser diodes. These excellent features are suitable for realizing an ultra-compact fibre lasers and amplifiers. In this section, an ultra-compact Bismuth-based *Q*-switched erbium-doped fibre laser (Bi-EDFL) using GO as a SA is proposed, with only 21 cm gain medium length and erbium ion concentration of 6300 ppm. Compared to conventional silica-based erbium-doped fiber laser (EDFL) with the same amount of erbium ions, the Bi-EDFL provides a higher attainable laser gain.

The configuration of the Bi-EDFL is the same as that shown in Figure 5.1, with only minor changes made to some of the optical components. The active medium of the Bi-EDFL is now a 21cm long Bi-EDF, with an erbium ion concentration of 6300 ppm as well as a core refractive index of about 2.03 and cladding refractive index of 2.02 at1550 nm. The peak absorption of the Bi-EDF is about 83dB/m and 133dB/m at wavelengths of 1480 and 1530 nm respectively. The Bi-EDF is pumped by a1480 nm

diode laser which is connected using a1480/1550 WDM. A tunable band- pass filter (TBF) is incorporated into the resonator to investigate the tunability of the laser.

Figure 5.25 shows the amplified spontaneous emission (ASE) spectra obtained at different pump powers. It can be seen that the Bi-EDF produces a broader ASE spectrum as compared to that obtained from conventional silica-based doped fibres. The ASE spectrum stretches from about 1490 nm to 1610 nm, forming a bandwidth of about 120 nm. At lower pump powers, the ASE spectra resemble a bell curve, rising slightly above plateauing and subsequently declining again. This is a result of the high erbium concentration, which re-absorbs the emissions of the ASE and producing emissions in the L-band region. As the pump power is increased, the conventional peak at 1530 nm for EDFs begins to be seen.

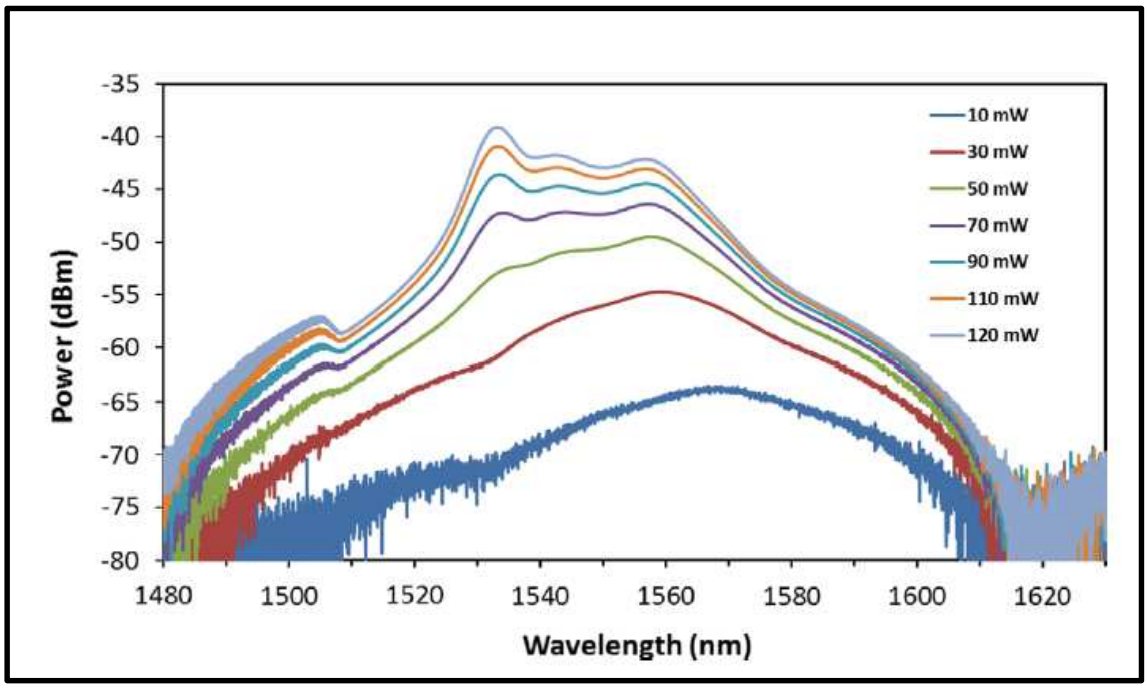

Figure 5.25: ASE spectra for 21 cm Bi-EDF at different pump powers.

The threshold for *Q*-switching is observed at about 65 mW, where it changes from continuous wave (CW) operation into *Q*-switched pulses by carefully adjusting the pump power and observing the changes on the oscilloscope. The average output power and pulse energy with the incident pump power is shown in Figure 5.26. The average

output power increases in almost linear manner, from about 0.03 to 0.11 mW as the pump power is increased from 65 to 118 mW. The slope efficiency, as measured from the graph is approximately 0.002. The pulse energy, on the other hand, increases at a slower rate at low pump powers., but rises sharply above a pump power of about 92 mW until the maximum value of 118 mW is achieved. At 92 mW, the pulse energy is about 3.2 nJ, and increases to almost 4.3 nJ at the maximum pump power. No pump saturation is observed at the maximum pump power. Higher pump powers and larger pulse energies can be achieved by having a higher powered pump laser, as well as by improving the quality of the GO absorber [51, 52] and by optimizing the laser resonator design, such as changing the coupling ratio and minimizing the resonator loss [53].

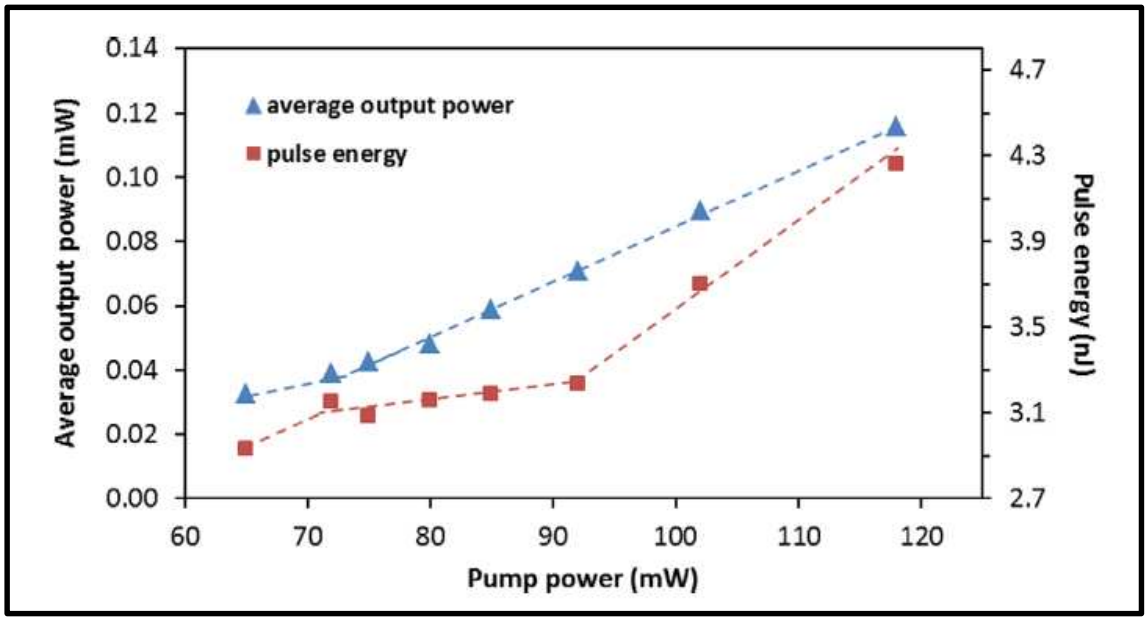

Figure 5.26: Average output power and pulse energy of the *Q*-switched Bi-EDFL as a function of incident pump power.

Figure 5.27 shows the pulse repetition rate and pulse widths as a function of the pump power. The repetition rate increases, from about 11.2 kHz to 27.2 kHz as the pump power is raised from 65 to 118 mW. This is because as the pump power increases, the power of the signal increases, causing the GO based SA to move towards saturation. The generation of the pulses is dependent on the saturation level of the SA. The pulse width of the generated pulses decreases as the pump power is increased, from a high

value of about 22.0 μs at a pump power of 65 mW, and dropping to about 7.7 μs at a pump power of 118 mW.

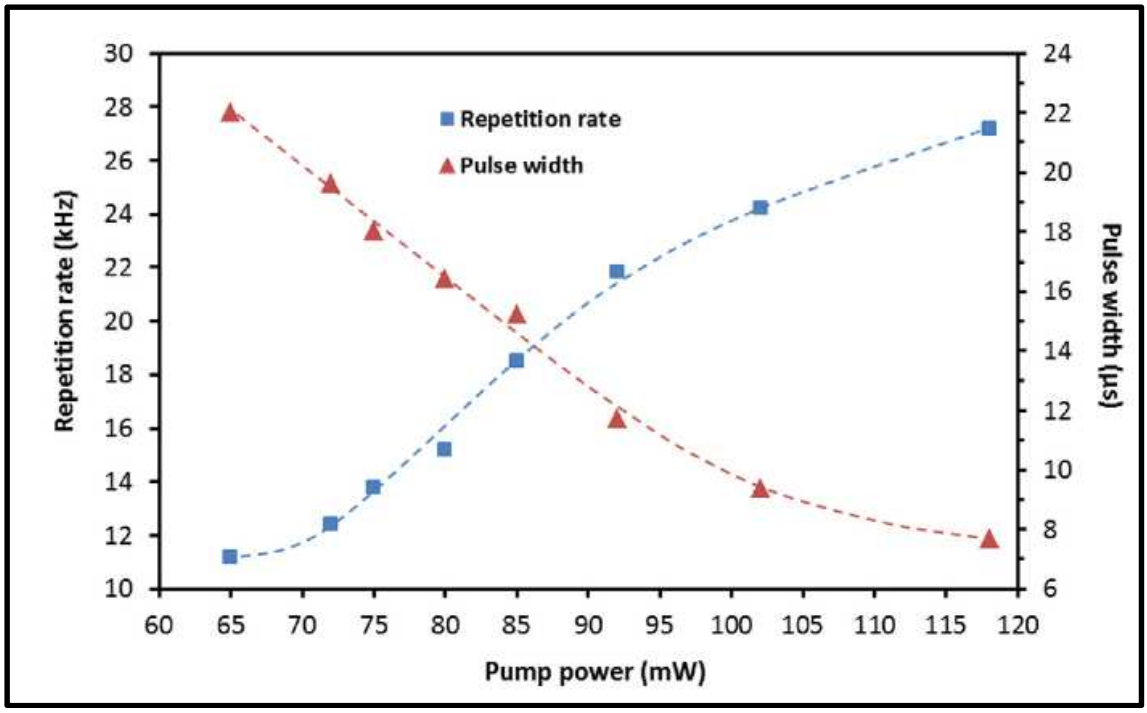

Figure 5.27: Repetition rate and pulse width of the *Q*-switched EDFL at the wavelength of 1566 nm.

Figure 5.28 shows the *Q*-switched pulse train and pulse profile under pump powers of 92 mW and 118 mW. As expected, the pulse narrows from 11.7 to 7.7 μs, corresponding to the behaviour of the *Q*-switched Bi-EDFL as observed in Figure 5.27. At the threshold, the pulse width is measured to be 22.0 μs. In the same manner, the repetition rate increases from 21.8 to 27.2 kHz for the same power range.

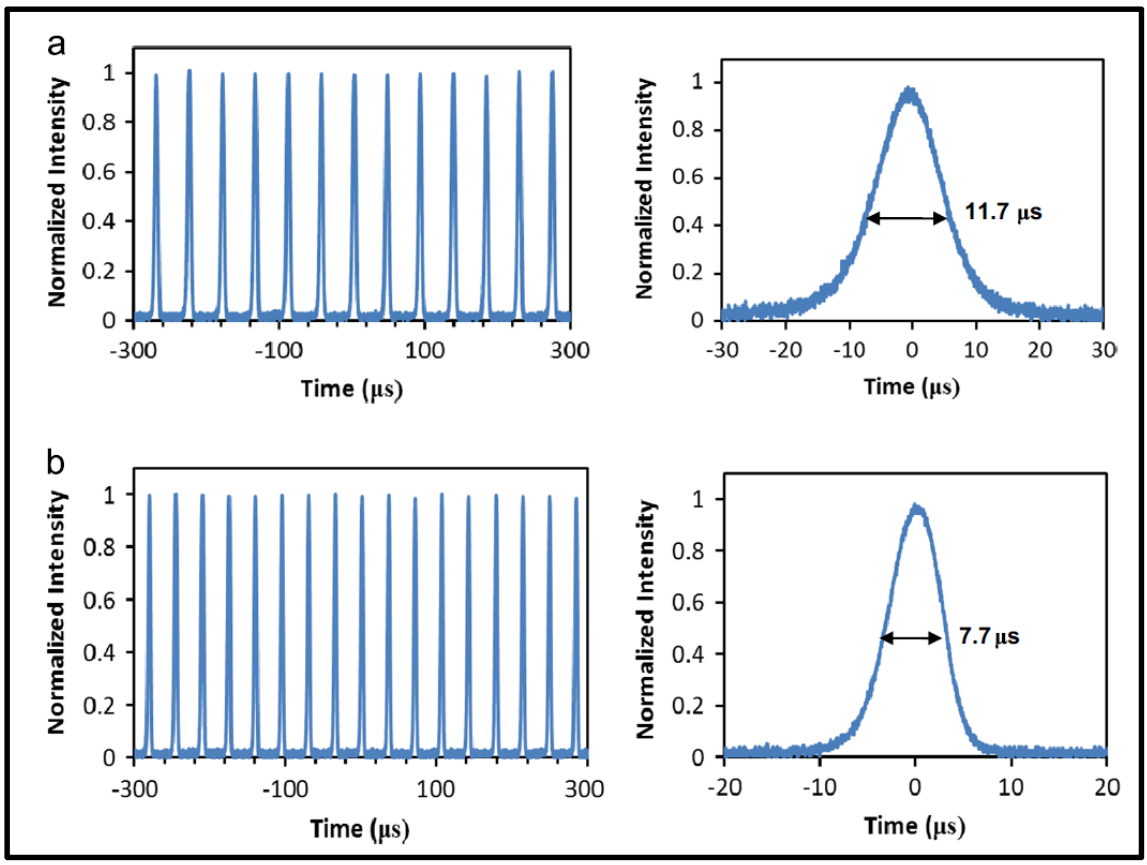

Figure 5.28: Pulse train and a single pulse profile of the *Q*-switched Bi-EDFL under (a) f = 21.8kHz, 92 mW and (b) f = 27.2 kHz, 118 mW of pump powers at 1555.6 nm.

Figure 5.29 shows the tunability of the *Q*-switched Bi-EDFL. Tunability is obtained by adjusting the TBF to the desired wavelength. It can be seen from the wavelengths generated, at a pump power of 92 mW, the laser has an average peak power of – 16.8 dBm, with a tuning range of approximately 1550 nm to 1564 nm. The full-width at half-maximum (FWHM) is about 0.1 nm, However, this range and average power is an example of the performance of the Bi-EDFL; higher peak powers can be achieved with higher pump powers, and the tuning range can be extended so as to cover the ASE spectrum.

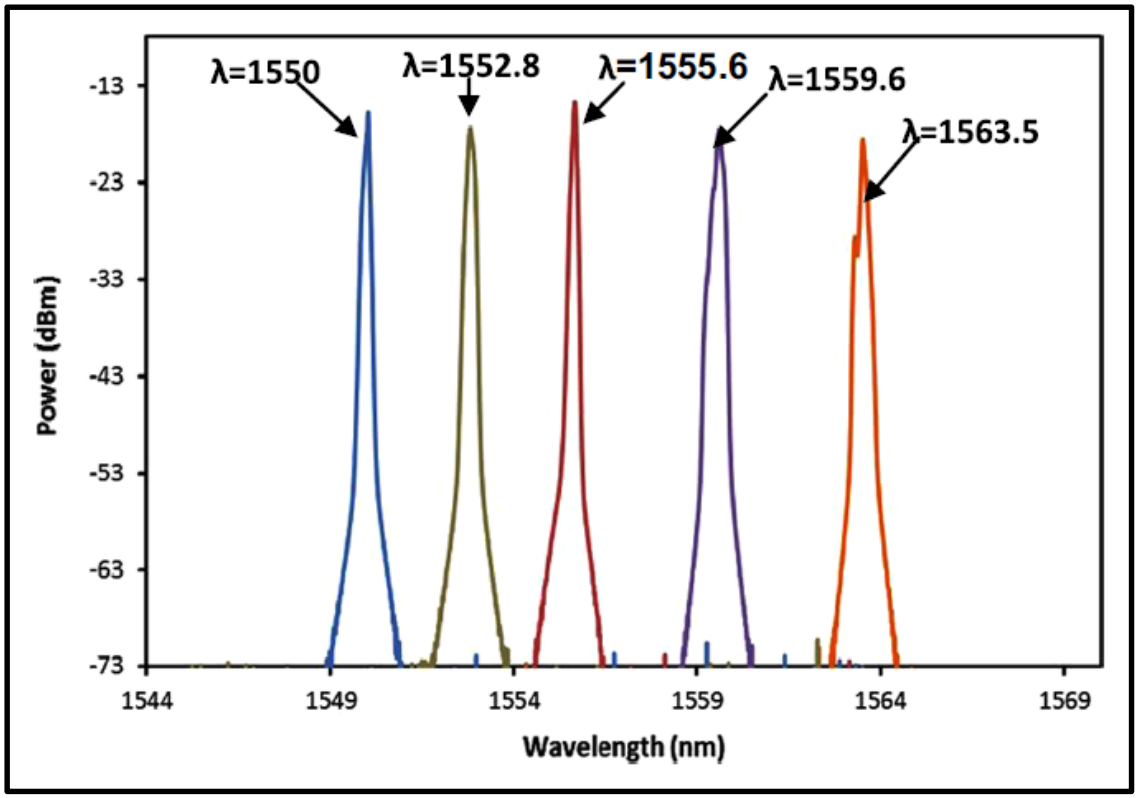

Figure 5.29: *Q*-switched laser spectra at different wavelengths tuned by a TBF at a fixed pump power of 92 mW. The base power is set at -73 dBm for clarity.

Figure 5.30 shows the spectrum obtained by using a Radio Frequency Spectrum Analyzer (RFSA). As can be seen from the figure, a fundamental pulse is obtained at 21.8 kHz, with a peak to pedestal ratio of about 31 dB. The pulse is observed to not change over a period of 60 minutes, thus demonstrating the stability of the output pulses. The inset also shows the generation of the harmonics in the pulsed laser, with the fundamental mode at 21.8 kHz and subsequent modes occurring at iterations of 21.8 kHz. The output of the *Q*-switched Bi-EDFL is highly stable, making it suitable for a multitude of applications that require stable, short pulses.

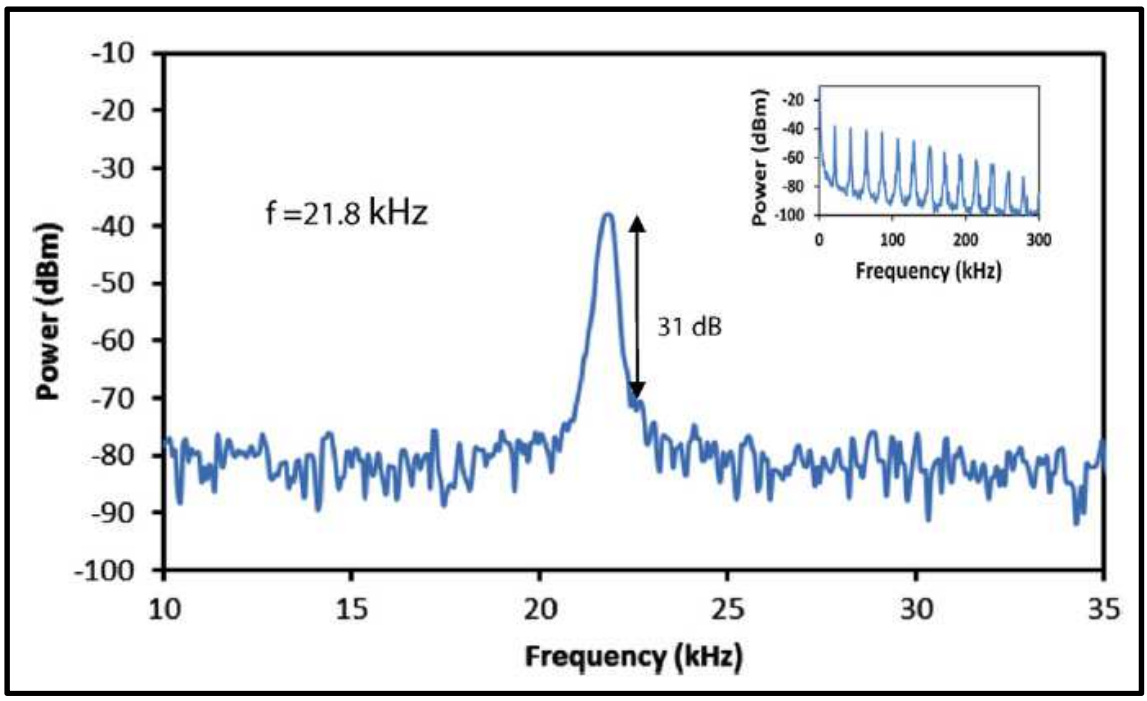

Figure 5.30: Spectrum of a *Q*-switched pulsed laser at 1556 nm as obtained from the RFSA at the pump power of 92 mW. The fundamental frequency of the pulse is 21.8 kHz. The inset shows the RF harmonics of the *Q*-switched pulsed laser. The RFSA is set at a span of 25 kHz, with a resolution bandwidth and video bandwidth of 300 Hz.

References

[1] Z. Jun-Qing, W. Yong-Gang, Y. Pei-Guang, R. Shuang-Chen, C. Jian-Qun, D. Ge-Guo, *et al.*, "Graphene-oxide-based Q-switched fiber laser with stable five-wavelength operation," *Chinese Physics Letters*, vol. 29, p. 114206, 2012.

[2] A. Martinez, K. Fuse, B. Xu, and S. Yamashita, "Optical deposition of graphene and carbon nanotubes in a fiber ferrule for passive mode-locked lasing," *Optics express*, vol. 18, pp. 23054-23061, 2010.

[3] S. O., *Principles of Lasers*, 4th ed. New York: Plenum Press, 1998.

[4] Z. Luo, M. Zhou, J. Weng, G. Huang, H. Xu, C. Ye, *et al.*, "Graphene-based passively Q-switched dual-wavelength erbium-doped fiber laser," *Optics Letters*, vol. 35, pp. 3709-3711, 2010.

[5] J. Zayhowski and P. Kelley, "Optimization of Q-switched lasers," *Quantum Electronics, IEEE Journal of*, vol. 27, pp. 2220-2225, 1991.

[6] R. Herda, S. Kivistö, and O. G. Okhotnikov, "Dynamic gain induced pulse shortening in< i> Q</i>-switched lasers," *Optics Letters*, vol. 33, pp. 1011-1013, 2008.

[7] R. Paschotta, R. Häring, E. Gini, H. Melchior, U. Keller, H. L. Offerhaus, *et al.*, "Passively Q-switched 0.1-mJ fiber laser system at 1.53 ?m," *Optics Letters*, vol. 24, pp. 388-390, 1999/03/15 1999.

[8] D. G. H. Ballard and G. R. Rideal, "Flexible inorganic films and coatings," *Journal of Materials Science*, vol. 18, pp. 545-561, 1983/02/01 1983.

[9] J. J. Kellar, *Functional Fillers and Nanoscale Minerals/New Markets/New Horizons*. Littleton, Colorado: Society for Mining, Metallurgy and Exploration, 2006.

[10] M. Dowell and R. Howard, "Tensile and compressive properties of flexible graphite foils," *Carbon*, vol. 24, pp. 311-323, 1986.

[11] Y. Leng, J. Gu, W. Cao, and T.-Y. Zhang, "Influences of density and flake size on the mechanical properties of flexible graphite," *Carbon,* vol. 36, pp. 875-881, 1998.

[12] R. A. Reynolds Iii and R. A. Greinke, "Influence of expansion volume of intercalated graphite on tensile properties of flexible graphite," *Carbon,* vol. 39, pp. 479-481, 2001.

[13] J. Liu, A. G. Rinzler, H. Dai, J. H. Hafner, R. K. Bradley, P. J. Boul, *et al.*, "Fullerene pipes," *Science,* vol. 280, pp. 1253-1256, 1998.

[14] R. H. Baughman, C. Cui, A. A. Zakhidov, Z. Iqbal, J. N. Barisci, G. M. Spinks, *et al.*, "Carbon nanotube actuators," *Science,* vol. 284, pp. 1340-1344, 1999.

[15] F. Hennrich, S. Lebedkin, S. Malik, J. Tracy, M. Barczewski, H. Rösner, *et al.*, "Preparation, characterization and applications of free-standing single walled carbon nanotube thin films," *Physical Chemistry Chemical Physics,* vol. 4, pp. 2273-2277, 2002.

[16] J. N. Coleman, W. J. Blau, A. B. Dalton, E. Munoz, S. Collins, B. G. Kim, *et al.*, "Improving the mechanical properties of single-walled carbon nanotube sheets by intercalation of polymeric adhesives," *Applied Physics Letters,* vol. 82, pp. 1682-1684, 2003.

[17] L. Berhan, Y. Yi, A. Sastry, E. Munoz, M. Selvidge, and R. Baughman, "Mechanical properties of nanotube sheets: Alterations in joint morphology and achievable moduli in manufacturable materials," *Journal of Applied Physics,* vol. 95, pp. 4335-4345, 2004.

[18] D. A. Dikin, S. Stankovich, E. J. Zimney, R. D. Piner, G. H. B. Dommett, G. Evmenenko, *et al.*, "Preparation and characterization of graphene oxide paper," *Nature,* vol. 448, pp. 457-460, 2007.

[19] A. Lerf, A. Buchsteiner, J. Pieper, S. Schöttl, I. Dekany, T. Szabo, *et al.*, "Hydration behavior and dynamics of water molecules in graphite oxide," *Journal of Physics and Chemistry of Solids,* vol. 67, pp. 1106-1110, 5// 2006.

[20] A. Buchsteiner, A. Lerf, and J. Pieper, "Water Dynamics in Graphite Oxide Investigated with Neutron Scattering," *J. Phys. Chem. B,* vol. 110, pp. 22328-22338, 2006/11/01 2006.

[21] F. Yang, Y. Liu, L. Gao, and J. Sun, "pH-sensitive highly dispersed reduced graphene oxide solution using lysozyme via an in situ reduction method," *The Journal of Physical Chemistry C,* vol. 114, pp. 22085-22091, 2010.

[22] D. C. Marcano, D. V. Kosynkin, J. M. Berlin, A. Sinitskii, Z. Sun, A. Slesarev, *et al.*, "Improved synthesis of graphene oxide," *ACS Nano,* vol. 4, pp. 4806-4814, 2010.

[23] D. Luo, G. Zhang, J. Liu, and X. Sun, "Evaluation criteria for reduced graphene oxide," *The Journal of Physical Chemistry C,* vol. 115, pp. 11327-11335, 2011.

[24] T. Stauber, N. Peres, and A. Geim, "Optical conductivity of graphene in the visible region of the spectrum," *Physical review B,* vol. 78, p. 085432, 2008.

[25] G. Sobon, J. Sotor, J. Jagiello, R. Kozinski, M. Zdrojek, M. Holdynski, *et al.*, "Graphene oxide vs. reduced graphene oxide as saturable absorbers for Er-doped passively mode-locked fiber laser," *Optics express,* vol. 20, pp. 19463-19473, 2012.

[26] Z. Sun, X. Lin, D. Popa, H. Yu, T. Hasan, F. Torrisi, *et al.*, "Wideband tunable, high-power, graphene mode-locked ultrafast lasers," in *The European Conference on Lasers and Electro-Optics*, 2011, p. JSII2_5.

[27] W. Fan, Q. Lai, Q. Zhang, and Y. Wang, "Nanocomposites of TiO2 and reduced graphene oxide as efficient photocatalysts for hydrogen evolution," *The Journal of Physical Chemistry C,* vol. 115, pp. 10694-10701, 2011.

[28] J.-L. Xu, X.-L. Li, Y.-Z. Wu, X.-P. Hao, J.-L. He, and K.-J. Yang, "Graphene saturable absorber mirror for ultra-fast-pulse solid-state laser," *Optics Letters*, vol. 36, pp. 1948-1950, 2011.

[29] Z. Ni, Y. Wang, T. Yu, and Z. Shen, "Raman spectroscopy and imaging of graphene," *Nano Research*, vol. 1, pp. 273-291, 2008.

[30] A. Ferrari, J. Meyer, V. Scardaci, C. Casiraghi, M. Lazzeri, F. Mauri, *et al.*, "Raman spectrum of graphene and graphene layers," *Physical Review Letters*, vol. 97, p. 187401, 2006.

[31] L. G. Cançado, A. Jorio, E. M. Ferreira, F. Stavale, C. Achete, R. Capaz, *et al.*, "Quantifying defects in graphene via Raman spectroscopy at different excitation energies," *Nano Letters*, vol. 11, pp. 3190-3196, 2011.

[32] L. Gui, W. Zhang, X. Li, X. Xiao, H. Zhu, K. Wang, *et al.*, "Self-assembled graphene membrane as an ultrafast mode-locker in an erbium fiber laser," *Photonics Technology Letters, IEEE*, vol. 23, pp. 1790-1792, 2011.

[33] G. Sobon, J. Sotor, J. Jagiello, R. Kozinski, K. Librant, M. Zdrojek, *et al.*, "Linearly polarized, Q-switched Er-doped fiber laser based on reduced graphene oxide saturable absorber," *Applied Physics Letters*, vol. 101, p. 241106, 2012.

[34] Y. Yap, R. M. De La Rue, C. Pua, S. Harun, and H. Ahmad, "Graphene-based Q-switched pulsed fiber laser in a linear configuration," *Chinese Optics Letters*, vol. 10, p. 041405, 2012.

[35] W. Cao, H. Wang, A. Luo, Z. Luo, and W. Xu, "Graphene-based, 50 nm wide-band tunable passively Q-switched fiber laser," *Laser Physics Letters*, vol. 9, p. 54, 2012.

[36] D. Popa, Z. Sun, T. Hasan, F. Torrisi, F. Wang, and A. Ferrari, "Graphene Q-switched, tunable fiber laser," *arXiv preprint arXiv:1011.0115*, 2010.

[37] H. Ahmad, M. Zulkifli, F. Muhammad, A. Zulkifli, and S. Harun, "Tunable graphene-based Q-switched erbium-doped fiber laser using fiber Bragg grating," *Journal of Modern Optics,* vol. 60, pp. 202-212, 2013.

[38] M. Ismail, F. Ahmad, S. Harun, H. Arof, and H. Ahmad, "A Q-switched erbium-doped fiber laser with a graphene saturable absorber," *Laser Physics Letters,* vol. 10, p. 025102, 2013.

[39] L. Zhang, Z. Zhuo, J. Wang, and Y. Wang, "Passively Q-switched fiber laser based on graphene saturable absorber," *Laser Physics,* vol. 22, pp. 433-436, 2012.

[40] W. J. Cao, H. Y. Wang, A. P. Luo, Z. C. Luo, and W. C. Xu, "Graphene-based, 50 nm wide-band tunable passively Q-switched fiber laser," *Laser Physics Letters*, vol. 9, p. 54, 2012.

[41] U. Keller, K. J. Weingarten, F. X. Kartner, D. Kopf, B. Braun, I. D. Jung, *et al.*, "Semiconductor saturable absorber mirrors (SESAM's) for femtosecond to nanosecond pulse generation in solid-state lasers," *Selected Topics in Quantum Electronics, IEEE Journal of,* vol. 2, pp. 435-453, 1996.

[42] Z. Luo, M. Zhou, D. Wu, C. Ye, J. Weng, J. Dong, *et al.*, "Graphene-induced nonlinear four-wave-mixing and its application to multiwavelength Q-switched rare-earth-doped fiber lasers," *Lightwave Technology, Journal of,* vol. 29, pp. 2732-2739, 2011.

[43] R. Paschotta, R. Häring, E. Gini, H. Melchior, U. Keller, H. Offerhaus, *et al.*, "Passively< i> Q</i>-switched 0.1-mJ fiber laser system at 1.53 μm," *Optics Letters*, vol. 24, pp. 388-390, 1999.

[44] E. Delevaque, T. Georges, M. Monerie, P. Lamouler, and J. F. Bayon, "Modeling of pair-induced quenching in erbium-doped silicate fibers," *Photonics Technology Letters, IEEE,* vol. 5, pp. 73-75, 1993.

[45] S. W. Harun, N. Tamchek, P. Poopalan, and H. Ahmad, "Double-pass L-band EDFA with enhanced noise figure characteristics," *Photonics Technology Letters, IEEE,* vol. 15, pp. 1055-1057, 2003.

[46] S. W. Harun, N. K. Saat, and H. Ahmad, "An efficient S-band erbium-doped fiber amplifier using double-pass configuration," *IEICE Electronics Express,* vol. 2, pp. 182-185, 2005.

[47] E. Kelleher, J. Travers, Z. Sun, A. Ferrari, K. Golant, S. Popov, *et al.*, "Bismuth fiber integrated laser mode-locked by carbon nanotubes," *Laser Physics Letters,* vol. 7, p. 790, 2010.

[48] R. Buczynski, H. Bookey, D. Pysz, R. Stepien, I. Kujawa, J. McCarthy, *et al.*, "Supercontinuum generation up to 2.5 μm in photonic crystal fiber made of lead-bismuth-galate glass," *Laser Physics Letters,* vol. 7, p. 666, 2010.

[49] S. Firstov, I. Bufetov, V. Khopin, A. Shubin, A. Smirnov, L. Iskhakova, *et al.*, "2 W bismuth doped fiber lasers in the wavelength range 1300–1500 nm and variation of Bi-doped fiber parameters with core composition," *Laser Physics Letters,* vol. 6, p. 665, 2009.

[50] I. Bufetov and E. Dianov, "Bi-doped fiber lasers," *Laser Physics Letters,* vol. 6, p. 487, 2009.

[51] Y.-W. Song, S.-Y. Jang, W.-S. Han, and M.-K. Bae, "Graphene mode-lockers for fiber lasers functioned with evanescent field interaction," *Applied Physics Letters,* vol. 96, p. 051122, 2010.

[52] H. Kim, J. Cho, S.-Y. Jang, and Y.-W. Song, "Deformation-immunized optical deposition of graphene for ultrafast pulsed lasers," *Applied Physics Letters,* vol. 98, p. 021104, 2011.

[53] J. J. Zayhowski and P. L. Kelley, "Optimization of <e1>Q</e1>-switched lasers," *Quantum Electronics, IEEE Journal of,* vol. 27, pp. 2220-2225, 1991.